İSTANBUL TECHNICAL UNIVERSITY ★ INSTITUTE OF SCIENCE AND TECHNOLOGY

ACCURATE DETERMINATION OF THE POTENTIAL ENERGY SURFACES AND THE MOLECULAR PROPERTIES FOR MHe^+ (M=Li, Na, K) COMPLEXES USING QUANTUM MECHANICAL TECHNIQUES

MS.SCI. Thesis by
Erol YILDIRIM, Chemist

Department : Chemistry

Program: Chemistry

Supervisor : Assoc. Prof. Dr. Mine YURTSEVER

MAY 2005

İSTANBUL TEKNİK ÜNİVERSİTESİ ★ FEN BİLİMLERİ ENSTİTÜSÜ

MHe^+ (M=Li, Na, K) SİSTEMLERİ İÇİN POTANSİYEL ENERJİ YÜZEYLERİNİN VE MOLEKÜL ÖZELLİKLERİNİN KUANTUM MEKANİK YÖNTEMLERLE HASSAS OLARAK HESAPLANMASI

YÜKSEK LİSANS TEZİ

Erol YILDIRIM

Anabilim Dalı: Kimya

Programı: Kimya

Tez Danışmanı: Prof. Dr Mine YURTSEVER

HAZİRAN 2005

İSTANBUL TECHNICAL UNIVERSITY ★ INSTITUTE OF SCIENCE AND TECHNOLOGY

ACCURATE DETERMINATION OF THE POTENTIAL ENERGY SURFACES AND THE MOLECULAR PROPERTIES FOR MHe^+ (M=Li, Na, K) COMPLEXES USING QUANTUM MECHANICAL TECHNIQUES

M.Sc Thesis by
Erol YILDIRIM, Chemist
(509031227)

Date of submission : 9 October 1996
Date of defence examination: 25 January 2005

Supervisor : Prof. Dr. Mine YURTSEVER
Members of the Examining Committee Ass. Prof. Fethiye Aylin KONUKLAR
Ass Prof. Nurcan TÜZÜN

JUNE 2005

ACKNOWLEDGEMENTS

I am grateful to my thesis supervisor, Prof. Dr. Mine YURTSEVER for her guidance, helpful comments and critisizm throughout this research**.**

The computer time provided by High Performance Computing Center at ITU is gratefully acknowledged.

JUNE 2005 Erol YILDIRIM

TABLE OF CONTENTS

LIST OF ABBREVIATIONS

LHe : Liquid Helium
SWF : Shadow Wave Functions
M : Metal
Rg : Rare Gas
PEC : Potential energy Curve
MCS : Monte Carlo Simulation
MP : Moller Plessed
CC : Coupled Cluster
CI : Configuration Interaction
CCSD : Coupled Cluster including single and double substitutions
QCISD : Quadratic Configuration Interaction including singlets, doublets
G03 : Gaussian 2003
DFT : Density Functional Theory
HF : Hartree Foch
UHF : Unrestricted Hartree Foch
B3LYP : Becke Three Parameter Hybrid Functionals
cc-pvXz :Correlation Consistent Polarized Valence X (X=double, triple…) Zeta basis set
CEPA : Coupled electron-pair approximation
IEPA : Independent electron-pair approximation
SCF : Self Consistent Field
SDTQ : Single, Double, Triple and Quadruple
BSSE : Basis Set Superposition Error
CPU : Central Processing Unit
H : Hamiltonian
Ψ : Wave function
ε : Eigenvalue
SAPT : Symmetry-adapted perturbation theory
PEC : Potential Energy Curve

LIST OF TABLES

LIST OF FIGURES

LIST OF SYMBOLS

D_e	: Dissociation energy
R_e	: Equilibrium bond length
H	: Hamiltonian
Ψ	: Wave function
ε	: Eigenvalue
E/N	: Electric field to neutral particle number density ratio
M^-	: Effective mass of the electron-containing bubble
$P_k(z)$	: Poisson distribution for pick-up of k particles
P_0	: Stagnation pressure
$\underline{P}$	: Perturbation Operator
S	: Overlep matrix
$\underline{T}$	: Cluster Operator
i, j, k, l,…	: Occupied spin-orbitals
r, s, t, u,...	: Virtual spin-orbitals
A, B, C	: Becke constants

SUMMARY

Laser ablation of in situ metals has recently made it possible to immerse a large number of different metal atoms and ions and small clusters of metal atoms in helium nanodroplets. Atoms and molecules are readily picked up by He droplets, and their spectra are detected through the use of either beam depletion following absorption or laser-induced fluorescence. Within the past three years, a wide variety of molecules, ranging from metal ions to large organic molecules and a number of van der Waals complexes and even large metal clusters, have been embedded in He droplets and studied either in infrared or in the visible region.

The complexes MHe^+ (M=Li, Na, K) are of great interest, since they are prototypes of a closed-shell singly charged cation interacting with a closed-shell atom. From a more applied point of view, the mobility of metal ions in He is important for the understanding of chemical plasmas, nucleation phenomena, phase transitions and structures formed in the atmosphere.

The purpose of the present study is to test the accuracy of the interaction potential functions for the diatomic complexes, MHe^+ (M=Li, Na, K), by using MPn, QCISD(T), CCSD(T), and DFT methods with highly accurate basis sets. Results for the potential well depths, zero point energies, dissociation energies, bound vibrational levels are presented. Some of the methods and basis sets employed here are computationally too expensive to study further growth of the metal-Helium clusters (MHe_n^+). From these studies, we determine the most suitable method for studying larger clusters and the level of accuracy of such calculations.

ÖZET

Lazer aşındırması metodu ile günümüzde birçok atom, molekül ve iyonun ultra soğutulmuş He nano damlacıkları içerisine sokulabilmekte ve oluşan kompleks yapıların absorpsiyon ve emisyon spektroskopilerinin alınması mümkün olmaktadır. Metal atomlarının ve iyonlarının He içerisindeki davranışlarının açıklanmasında teorik ve deneysel metodlar yoğun olarak kullanılmaktadır. Bunun yanı sıra alkali metal atom ve iyonlarının soygazlarla oluşturdukları kompleksler de son yıllarda birçok teorik çalışmaya konu olmuştur. Bu atom kümeleri aralarındaki etkileşimler yoğun madde ve gaz fazı arasında bir geçiş olduğundan nükleasyon kavramı, faz değişimi, atmosferin üst katmanlarındaki molekül yapıları ve birçok reaksiyonun anlaşılması açısından önemlidir.

Bu çalışmanın amacı MHe^+ (M=Li, Na, K) iki atomlu sistemleri için potansiyel enerji eğrilerinin ve moleküler özelliklerinin (disosiyasyon enerjilerinin , titreşim seviyelerinin) çeşitli kuantum mekanik yöntemler (MPn, QCISD(T), CCSD(T)) ve yüksek bazlar kullanılarak hesaplamaktır. Buradan elde edilen sonuçlar metal içeren çok atomlu helyum yığınlarının yapılarını ve özelliklerini anlamak üzere yapılacak hesaplarda kullanılacak, hesaplama zamanı bakımından en uygun ve yüksek hassasiyetteki yöntem ve baz seçimini oluşturmak için büyük önem taşımaktadır.

1. INTRODUCTION

Since its discovery in 1954 [1] matrix isolation in crystals has become a powerful experimental technique, which is particularly useful in studies of transient species, such as atoms, molecular radicals, and ions [2-4]. Seeded supersonic beams is another technique which have also been used to cool free molecules, and to produce free molecular complexes and clusters. Recently a combination of the two techniques led to the development of a new experimental approach, the isolation of species in ultracold (T=0.37–0.15 K) helium droplets, which are made up of 10^3 to 10^8 helium atoms [5-9]. The fluid helium drops can readily pick up atoms and molecules and can form complexes from the species embedded in their interiors, or on their surfaces, thereby providing unique experimental opportunities. Extensive experiments conducted in the last 10 years have demonstrated helium droplets to be the ultimate matrix for the 'ultracold' experiments. They are characterized by extremely low temperatures, little matrix broadening, and offer unique possibilities to synthesize new molecular complexes [10].

Superfluid ^{4}He exhibits a range of unusual phenomena, such as a vanishingly small viscosity, very high heat conductivity (30-times greater than copper) and many other unusual effects, such as the He fountain, film flow and creep, and quantized vortices. The fundamental differences in the behavior of classical liquids or solids and the quantum liquid helium, respectively, determines the extraordinary differences in their properties as spectroscopic matrices.

Presumably there have been many proposals in the past to use the optical spectroscopy of foreign species as a microscopic probe for liquid helium; after all, spectroscopic techniques have found widespread applications in other areas of condensed matter physics. However, until recently, these studies were not feasible owing to the extremely low equilibrium solubility of single molecules of any foreign species in liquid helium.

Impurities quickly coagulate to form clusters that either rise to the surface or fall to the bottom of the reaction vessel [11]. Contemporary methods of immersing foreign atoms into bulk liquid helium usually involve laser induced ablation of metals into the liquid [12-14]. This method makes it possible to obtain rather large transient concentrations of "metal atoms" in the liquid, however, to date the successful implantation of species other than metals, in particular of intact molecules, into bulk liquid helium has not been possible. One recent experimental development involves first embedding the foreign species inside large helium droplets formed in a pulsed beam and then directing the beam at the surface of the helium bath [15]. The discovery [18] that also ions can be captured inside helium nanodroplets opens the way to a new class of experiments which will be a unique opportunity for testing the accuracy of the microscopic theories.

Laser ablation of in situ metals has recently made it possible to immerse a large number of different metal atoms and ions and small clusters of metal atoms in liquid helium [LHe] and thus study their absorption and emission spectra in the visible region. Atoms and molecules are readily picked up by large ($N = 10^3$ atoms) He droplets, and their spectra are sensitively detected through the use of either beam depletion following absorption or laser-induced fluorescence [5].

The study of charged impurities in superfluid ^{4}He has a long history as a way to probe different aspects of superfluidity. As an example, the experimental verification of the Landau critical velocity is mentioned [40]. A charged impurity is expected to strongly modify the local environment of the liquid. Some impurities like an electron or He^- are believed to form a cavity as an effect of the repulsion which arises from the Pauli Exclusion Principle. Other impurities like the alkali ions should form a region of increased density due to electrostriction that means local density has been estimated to be so large that some kind of solid order is expected to be present. This is the so-called snowball model that Atkins [19] developed and that has been widely used to interpret the experimental data. On the basis of this phenomenological model, the snowball does not depend on the specific ion one is considering. The presence of the snowball is at the basis of the explanation of the very low mobility of a positive ion, which is seen experimentally, as compared with that of a neutral species such as ^{3}He. Experimentally, the mobility is known to depend on the identity of the core ion. Next, ions are useful

probes on a microscopic scale of the properties of superfluid helium and, in the past decades, a considerable effort has been devoted to the study of the metal ion-He complexes [16,17]. Whereas electrons form bubbles of 34 A° diameter [20,21,22], positive ions are surrounded by many He atoms that are strongly compressed as a result of electrostriction and smaller structures are formed. The resulting core is thought to be solid, with a diameter of 11A° containing about 35 He atoms, and is referred to as a snowball as mentioned [23-25]. The large effective mass of the electron-containing bubble, which has been found to be about $M^- = (243)m_4$ (where m_4 is the mass of a ^{4}He atom), is due entirely to hydrodynamic backflow effects [26]. The smaller mass of the snowballs, $M^+ = (43.6)\, m_4$, is mainly that of the solid core.

The large (34°A) diameter of the bubble formed around an electron can be explained by the strong Pauli-principle exchange repulsion between the electron and the surrounding He atoms and can be seen for all anions [20,21]. These models mentioned has been adapted to snowball structures to explain similar cavities formed by excited He atoms also [27-29], by metal atoms [30-35], and by alkaline earth ions [25] in LHe. In these cases the radii of the bubbles are, however, smaller (5 to 6 A°) because of attractive-electrostatic and polarization forces with the ion cores. The properties of these bubbles can be calculated by minimization of the total energy of the system. The bubble model can qualitatively explain most of the spectroscopic observations. The excitation spectrum of a bubble with an enclosed electron or an atom can be calculated using the Frank-Condon principle, assuming that the shape and width of the bubble are unchanged during the transition. The lines are broadened as a result of a coupling of the excited electronic state to bubble vibrations [21]. The line shape may also be calculated using static line-broadening theory [36]. Because the equilibrium radius of a bubble surrounding an excited atom is larger than it is in the ground state, the atomic absorption lines are expected to be broader and to have a large blue shift relative to the free atom. Emission occurs after relaxation to the lowest energy state within the expanded bubble; the corresponding spectral lines have a smaller blue or even a red shift and are usually narrower. On the other hand, the quantitative explanations of the shifts and line shapes of the spectra generally demand the fitting of the semiempirical model parameters to the particular spectrum.

The bubble model assumes that the pressure work and the surface energy terms at dimensions comparable to interatomic distances can be calculated from the corresponding macroscopic quantities. The bubble model breaks down and snowball model is used for positive charges inside LHe. In this case, the very strong polarization forces attract the He atoms to such an extent that several layers become solid. For neutral species other than ground-state alkali atoms, the attractive forces are much weaker. Nevertheless, a substantial increase of He density has been predicted theoretically [37]. Only the most recent theories of embedded molecules also include the effects of the anisotropic interaction potential [38]. Calculations with anisotropic potentials show a strong angular dependence of the density profile for neutral molecules in the He [39].

Nearly all metals from the first to the fourth periods of the periodic system have been investigated via their dispersed fluorescence or by laser induced fluorescence (LIF) spectroscopy [12,14,41,42]. The visible spectra of the molecular dimers and trimers have also been reported for Ag_2, Ag_3 [43], Na_2, Li_2 [44], Ca_2, and Cu_2 [45] in L^4He. The ion mobilities in LHe were measured for Mg^+, Ca^+, Sr^+, Ba^+, Ag^+, Au^+, Na^+ [46,16].

The M^+-Rg complexes (M=Alkali metal, Rg=Rare gas atom) are of great interest from a fundamental point of view, since they are prototypes of a closed-shell singly charged cation interacting with a closed-shell atom. The interaction potentials of these species are important for calculating the transport properties of the cations in a bath of the inert gas, which is of consequence in understanding the mobility of ions in plasma discharges and the far reaches of the Earth's atmosphere [47, 48]. Consequently, it is not surprising that a number of studies have been performed on such species. These cover theoretical studies [49-56], mobility [57,58] and beam studies. All of these studies give rise to information on the potential energy curve. As such, variety of experimental and theoretical methods, with such studies yielding information on the short- and long-range portions of the potential energy curve [50].

The first systematic general study of alkali ions in superfluid ^4He based on a microscopic variational theory. It is found that the density profile around the ion has a very strong peak corresponding to a first shell of atoms and this is in qualitative

agreement with what is expected on the basis of the snowball model. In other respects, results are in profound disagreement with that model. It is said that the picture of a snowball is a reasonable one in the case of K^+ and Na^+ get a microscobic description for snowball model [59]. It is clear that each ion has its own environment in terms of the number of atoms in the first shell of solvation by He atoms, of the degree and the kind of local order, and of the degree of localization of these atoms. Not only Group 1 cations like K^+, Na^+, and Cs^+ [60] but also Group 2 cations like Be^+ and Mg^+ are studied with variational techniques by employing shadow wave functions (SWF) which was later improved to allow for the anisotropic correlations between ^{4}He atoms and the ion. The first shell of ^{4}He atoms around the ions has always a well defined solidlike structure, which is remarkably different for each ion but it does not depend on the ^{4}He system (bulk liquid or cluster). The first microscopic computations of these systems have been performed with the SWFs and were devoted to the study of some alkali ions in bulk liquid He (Li^+, Na^+, K^+ and Cs^+) [59] and in He nanodroplets ($K^+$and Na^+) [40].

Mobility measurements on the alkali ions by Glaberson and Johnson [17] give an estimate of the snowball radius of 8.35 Å for K^+ and 8.4 Å for Cs^+ and the mobility is seen to decrease as the atomic number of the core ion increases. On the other hand, for the alkali earth ions (Ca^+, Sr^+, Ba^+) the reverse trend was observed [40, 59].

The spectroscopic constants for the ground and selected low-lying electronic states of the transition metal-noble gas ions have been determined at the modified coupled-pair functional level of electron correlation treatment. There is a strong correlation between the binding energy and bond length, since the bonding is predominantly electrostatic (charge-induced dipole). In general, calculated binding energies are about 20% less than the experimental values due to limitations in the level of theory used in the past studies [61].

The Tang–Toennies model [55] was modified to predict the potentials for ion–atom systems [64]. First order SCF energies are used to describe the repulsive potential. The long range second order induction and dispersion potential terms up to R^{-10} are either taken from ab initio calculations or estimated and each term is appropriately damped. The potentials for Li^+, Na^+, K^+, F^-, and Cl^- interacting with He, Ne, and Ar are found

to agree well with both theoretical and experimental data within the expected errors. For comparison with the model new ab initio calculations have been performed for Na^+–Ar and the results are in good agreement (<10%) with the model predictions.

Before Koutselos [62] experiments, which were important to be experimental work on ion rare gas complexes, it is shown that very reliable results can be obtained by neglecting the correlation of the helium charge density, and, simultaneously, accounting for the polarization of the lithium density. It is proposed that the method be applied to heavy alkali-ion-rare-gas molecules [63].

Using various recently proposed interaction potentials for the $LiHe^+$ system, elaborate calculations of the mobility, longitudinal, and transverse diffusion coefficients of Li^+ swarms in helium have been made by Monte Carlo simulations (MCS) [64]. In addition, the transverse diffusion coefficients for this ion–neutral-atom pair have been experimentally measured with total errors of ±3%. The close agreement of the experimental results with those of in literature [50] as well as the MCS reproduction of all three transport coefficients using the interaction potential proposed by Larsen [65].

In comparison, the more recent potentials of Ahlrichs [66] and of Koutselos, Mason, and Viehland [62] did not reproduce the experimental data. Recently, ab-initio quantum dynamics with very weak van der Waals interactions that is between Li_2 ($1\Sigma g+$) and He_2 cluster [67] was studied after collisional cooling of Li_2 ($1\Sigma g+$) by 'ultracold' collisions with an ^4He buffer gas. Advanced ab initio calculations were carried out at various levels of treatment of correlation forces, for the orientation and distance dependence of the interaction between a helium atom and the ionic core. Although the initial works were mostly on $LiHe^+$, later $NaRg^+$ complexes have also received some attention and they were studied by using ab initio techniques [68]. The $LiHe^+_n$, the $NaHe^+_n$, and the $MgHe^+_n$ complexes with n=1, 2, 3, 4 were studied using ab initio calculations with the MP2/6-311+G (3df, 3pd) method. The complexes are found to be stable. For the n=1 complexes, the calculations performed are in good agreement with the previous results [69]. Interatomic potential energy curves are presented by Soldan for the $Na\text{-}Rg^+$ and $Li\text{-}Rg^+$ (Rg=He, Ne and Ar) cationic complexes [68]. The basis set superposition error corrected curves for the diatomic systems are calculated at the CCSD(T)/ aug-cc-

pVQZ/5Z level of theory which is the most accurate method used for these systems up to now.

The purpose of the present study is to calculate the accurate the interaction potential energy curves for the diatomic complexes, MHe^+ (M=Li, Na, K), by employing the post-HF (Hartree-Fock) techniques like second and fourth order Moller-Pleset perturbation theories (MPn), Coupled-Cluster methods (CCSD(T)) , Quadratic Configuration Interaction method (QCISD(T)) and Density Functional Theory (DFT) methods with large basis sets. Results for the internuclear separations, dissociation energies and bound vibration levels are presented. Some of the methods and basis sets employed here are computationally too expensive to study further growth of the charged metal-helium clusters (MHe_n^+). From these studies, we determine the most suitable method for studying larger clusters and the level of accuracy of such calculations.

2. THEORY

2.1. Alkali ion-rare gas complexes

The M^+-Rg complexes, where M is an alkali metal and Rg is an inert gas, are prototypes of a closed-shell, singly-charged cation interacting with a closed-shell atom. As such, they have been studied by a variety of experimental and theoretical methods, with such studies yielding information on the short- and long-range portions of the potential energy curve [49,50]. The interaction potentials of these species are important for calculating the transport properties of the cations in a bath of the inert gas, which is of consequence in understanding the mobility of ions in plasma discharges and the far reaches of the Earth's atmosphere [68] and for understanding of nucleation phenomena, phase transitions, cluster-specific reactions and interactions of metal complexes [69].

2.2. Elements and molecules in the He

There have been many proposals in the past to use the optical spectroscopy of foreign species as a microscopic probe for liquid helium; after all, spectroscopic techniques have found widespread applications in other areas of condensed-matter physics. However, until recently, these studies were not feasible owing to the extremely low equilibrium solubility of single molecules of any foreign species in liquid helium. Impurities quickly coagulate to form clusters that either rise to the surface or fall to the bottom of the reaction vessel [11]. Contemporary methods of immersing foreign atoms into bulk liquid helium usually involve laser induced ablation of metals into the liquid [12, 13, 30]. This method makes it possible to obtain rather large transient concentrations of “metal atoms” in the liquid, however, to date the successful implantation of species other than metals, in particular of intact molecules, into bulk liquid helium has not been possible. One recent experimental development involves first embedding the foreign species inside

large helium droplets formed in a pulsed beam and then directing the beam at the surface of the helium bath [15].

2.3. Special Properties of the ultra cold He

Isolation in a solid matrix usually involves a co-deposition of the matrix and solute species. Once the matrix is prepared, isolated species may be ionized or photodissociated to produce ions or radicals, respectively. Thus matrix isolation provides a versatile tool to study a wide variety of these transient species [2,3,5,71]. Usually it is possible to obtain a rather large optical density of isolated species and maintain them for long times of several hours and even days which facilitates the straightforward application of the Fourier transform infrared and other optical spectroscopic techniques, such as Raman scattering. The relatively strong interaction of the matrix with its surrounding localizes the solute species and provides stability within the matrix, however broadening of the spectral lines may occur owing to the number of different sites which the solute molecules can occupy. A solute molecule usually does not perfectly fit into a void within the matrix crystal and it leads to a range of configurations of its nearest neighbor matrix environment. Moreover, the mobility of the particles in a solid matrix is low and ill defined, which makes it difficult to control experiments involving two or more species [25].

The situation is quite different for a molecule inside liquid helium (LHe). Because of their large quantum mechanical delocalization, the helium atoms in the vicinity of the molecule are able to adopt a unique and largely delocalized configuration corresponding to the ground state. Thus, in comparison to a molecule in a solid matrix, which is often described as a molecule in a “crystal field”, liquid helium gently adapts itself to the solute giving rise to a void perfectly tailored to a particular molecule. Moreover, helium is an ideal matrix material since it is completely transparent in the entire spectral range from the far IR to the vacuum UV. On the other hand, in its superfluid state, molecules may move freely in the LHe, thus remain highly mobile even close to absolute zero [26, 73]. Because of its high mobility and droplet size [74], LHe had a limited usage as a spectroscopic matrix for many years. Many attempts to isolate molecules have failed because of an uncontrolled precipitation of the solute species. With the advent of

helium-droplet beam technology it has become possible to isolate single molecules or certain numbers of the molecules inside a finite sized free helium droplet. The confinement of single molecules inside or on the surface of the free droplets avoids any problems with their aggregation or precipitation on container walls. At the same time the droplets provide a number of additional unique experimental opportunities. The droplet may be viewed as a "personal" nanocryostat for each individual molecule, "powered" by the evaporative cooling of the droplet material. The technological trade-off is that the experiments involve molecular beams of droplets inside a high-vacuum apparatus. Thus the lifetime of a single-droplet nanocryostat is only the typical time of their flight through the apparatus which is in the range of a few milliseconds. In addition, the optical density in the beam is far too low to apply directly most absorption spectroscopic methods and the application of laser light sources and special techniques for detection gain importance.

Recently, high spectroscopic resolution comparable to the gas phase can be achieved to study helium or rare gas droplets. Isothermal low-temperature environment is maintained by evaporative cooling at T =0.37 K (^{4} He droplets) or 0.15 K (^{3}He droplets) which are lower than possible temperatures in most solid matrices.Thus the helium-droplet technique combines the benefits of both the gas phase and the classical matrix-isolation techniques. Most importantly; the superfluid helium facilitates binary encounters and absorbs the released binding energy upon recombination. Thus the droplet can be viewed as an isothermal nanoscopic reactor, which isolates single molecules, clusters, or even single reactive encounter at ultralow temperatures [72].

2.4. Structures formed by charged particles in the He

The study of charged impurities in superfluid ^{4}He has a long history as a way to probe different aspects of superfluidity. A charged impurity is expected to strongly modify the local environment of the liquid. Some impurities like an electron or He^- are believed to form a cavity as an effect of the repulsion which arises from the Pauli exclusion principle. Electrons also form bubbles of 34 A° diameter [20-23], positive ions are surrounded by many He atoms that are strongly compressed as a result of electrostriction. The resulting core is thought to be solid, with a diameter of 11A°

containing about 35 He atoms, and is referred to as a snowball [24, 25]. The large effective mass of the electron-containing bubble, which has been found to be about

$M_- = (243)\ m_4$ (where m_4 is the mass of a ^{4}He atom), is due to hydrodynamic backflow effects [26]. The smaller mass of the snowballs, $M_+ = (43.6)\ m_4$, is mainly that of the solid core.

The large diameter of the bubble formed around an electron, has also been adapted to explain similar cavities formed by excited He atoms [27,28,29], by metal atoms [30-35], and by alkaline earth ions [24] in LHe. In these cases the radii of the bubbles are, however, smaller (5 to 6 A°) because of attractive-electrostatic and polarization forces with the ion cores. The properties of these bubbles can be calculated by a minimizing of the total energy of the system. The bubble model can qualitatively explain most of the spectroscopic observations. The excitation spectrum of a bubble with an enclosed electron or an atom can be calculated using the Frank-Condon principle, assuming that the shape and width of the bubble are unchanged during the transition. The lines are broadened as a result of a coupling of the excited electronic state to bubble vibrations [36]. The line shape may also be calculated using static line-broadening theory [21]. Because the equilibrium radius of a bubble surrounding an excited atom is larger than it is in the ground state, the atomic absorption lines are expected to be broader and to have a large blue shift relative to the free atom. Emission occurs after relaxation to the lowest energy state within the expanded bubble; the corresponding spectral lines have a smaller blue or even a red shift and are usually narrower. On the other hand, the quantitative explanations of the shifts and line shapes of the spectra generally demand the fitting of the semiempirical model parameters to the particular spectrum.

As a result, impurities like the alkali ions should form a region of increased density due to electrostriction that means local density has been estimated to be so large that some kind of solid order is expected to be present. This is the so-called snowball model that Atkins [19] developed and that has been widely used to interpret the experimental and theoretical data. On the basis of this phenomenological model, the snowball does not depend on the specific ion. The value of the radius of the snowball is about 6.5 Å and about 40 He atoms are involved in this structure. The presence of the snowball can be

explained by the very low mobility of a positive ion compared to that of a neutral species such as ^{3} He. Experimentally, the mobility is known to depend on the identity of the core ion. Mobility measurements on the alkali ions by Glaberson and Johnson [17] give an estimate of the snowball radius of 8.35 Å for K^+ and 8.4 Å for Cs^+ and the mobility is seen to decrease as the atomic number of the core ion increases. On the other hand, for the alkali earth ions [Ca^+, Sr^+, Ba^+] the reverse trend was observed. Although there are improved theories [75], there is still a substantial lack of microscopic theories for treating realistically a local solid order at the same time as the liquid far from the ion [76]. Therefore, questions like which kind of solid order is present, whether it depends on the chemical species of the ion, and which is the effect of the local modification of the liquid environment on the effective mass of the ion are not answered yet. The local symmetry around an ion is important in the treatment of nuclear spin polarization, which is the object of recent experiments [59]. To shed light on the questions above, there is still a great interest to study the properties of molecules which are captured inside a cluster of He atoms [5].

2.5.Doping Liquid He Nanodroplets

2.5.1.Droplet Sources

Macroscopic droplets of helium, which appear as a fog upon rapid Joule-Thomson cooling of the gas, were first observed about 100 years ago [77]. More recently helium fogs have been generated by a piezelectric transducer, placed few milimeters below the surface of liquid helium [78]. Other experiments involve laser [79] or magnetic field assisted [80] levitation of single very large droplets, about 10 μm to 2 cm in diameter in vacuum. Large positively charged helium droplets have been produced by field ionization of a liquid in an electrostatic-spray experiment [81]. Another recent approach is the formation of helium droplets by a pulsed expansion of cold helium gas into bath helium cryostat [15]. Although of considerable interest these methods have not yet been used for matrix isolation purposes.

At present all molecular spectra in liquid helium have been obtained in helium droplets produced in free jet expansions, mostly of gaseous He but also in a few cases in

expansions of the liquid. Helium-droplet production in gas expansions was first demonstrated by Becker in 1961 [82].

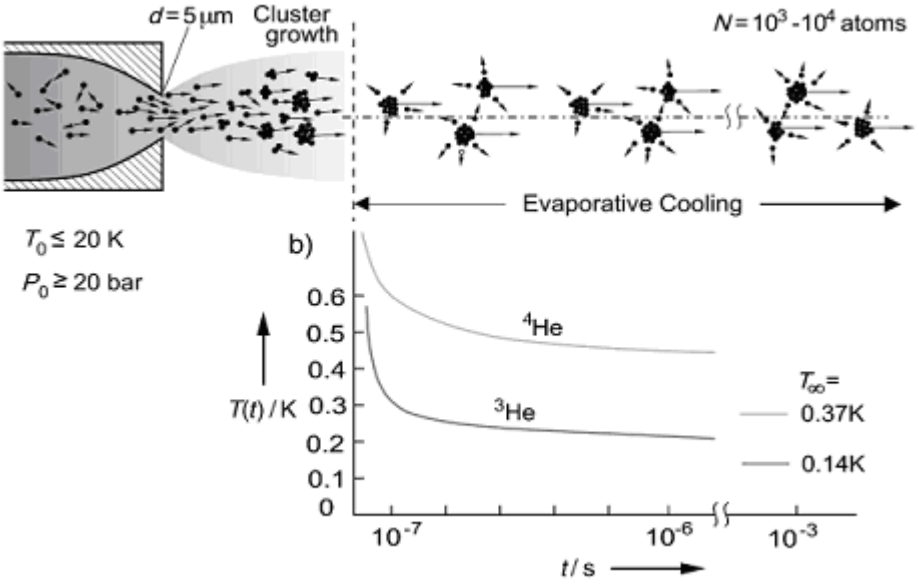

Figure 2.1: Schematic representation of the processes leading to the formation and subsequent cooling of helium droplets in a gas expansion. b) Calculated dependence of the droplet temperature on time for ^{4}He and ^{3}He droplets after they have left the cluster-growth region in the expansion and are traveling in vacuum

Beams containing either ^{4}He and ^{3}He droplets or mixed droplets with between several hundred and 10^4 atoms are readily produced today by expanding the gas at a high source pressure P_0=20-100 bar and a low source temperature T_0=20-5 K, through a tiny nozzle of several microns diameter or a narrow thin-walled orifice into vacuum (Figure 2.1) [5, 7, 83, 84]. The properties of droplets formed in continuous beams obtained by expansion through a 5-μm diameter orifice are now well characterized [85-87]. Recently pulsed (30-50 microsecond) beams of helium droplets with comparable properties have been developed with 1000-times larger peak droplet intensities [88].

2.5.2.Doping Process

As shown in Figure 2.2 the droplets are doped by passing the droplet beam through a pick-up cell filled with the vapor of the chromophore. This technique was first introduced and used for spectroscopic experiments with heavier noble-gas clusters by Scoles [89]. Initially it was not clear whether this technique could be used for helium droplets, because early experiments in the group of Gspann [90] were interpreted as indicating that because of their superfluid state He droplets are transparent for foreign species, such as Xe and Cs atoms. Only later did careful mass spectroscopic experiments [91] in Göttingen demonstrated that He droplets have the unique ability to pick up any species with which they collide.

The generation of a plasma by focusing the laser onto the target material leads inevitably to a certain degree of ionization of the evaporated material. Ions produced in this way have been utilized in several experiments for, e.g., the generation of beams of metal cluster ions. The isolation of ions in helium droplets has several interesting perspectives. Charged atoms such as, alkaline earth atoms, are interesting with respect to interaction with a helium environment [14]. In particular, the formation of ‘‘bubble’’ and ‘‘snowball’’ structures has been an issue. On the other hand, the isolation of cluster ions as well as of molecular ions opens up the possibility of studying these entities at millikelvin temperatures.

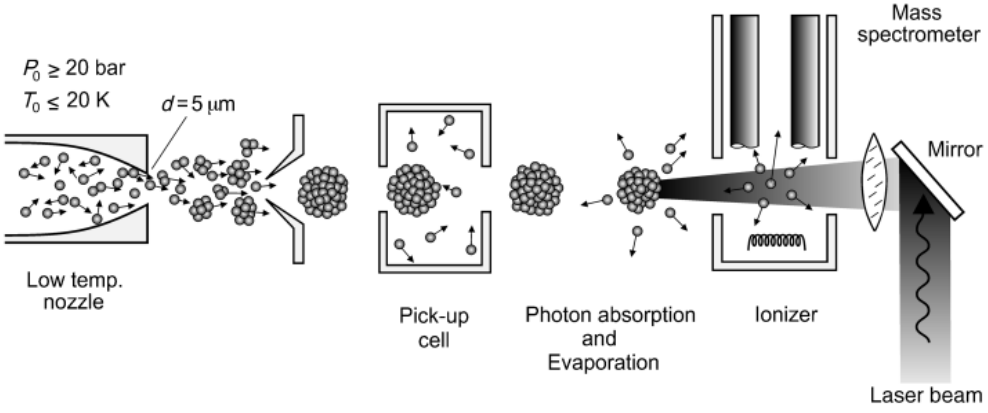

Figure 2.2: Schematic representation of the laser-depletion apparatus used for the pick-up and depletion spectroscopy of molecules inside helium droplets [10]

Low vapor pressure species, such as metals or large organic molecules, are sublimated in a heated cell. Since the pick-up cross section is close to the geometrical cross sections of the droplet, that is, typically of the order of 5000 $Å^2$ or larger, a vapor pressure of about 10^{-6}-10^{-5} mbar is sufficient for picking up of a single particle. Therefore, even species with low volatility, for example, amino acids [92] or refractory compounds and metals may be successfully embedded. Pulsed droplet beams [88] open up the possibility to use laser ablation and other pulsed techniques to pick-up low volatility species, such as larger biomolecules, or unstable transient species, such as radicals and ions [93]. Recently, laser ablation of copper has been used to dope helium droplets obtained in the pulsed nozzle beam expansion over the liquid helium surface [15]. Laser ablation of Mg close to the continuous helium droplet source, was used to form helium droplets doped with Mg atoms and Mg^+ ions [18].

The pick-up process leads to a decrease in the initial droplet size, a result of the kinetic energy and the internal energy of the impacting molecule, as well as its chemical potential, all of which are transferred to the droplet and lead to a subsequent rapid evaporation of He atoms. As a rule of thumb 1 eV of heat released corresponds to the evaporation of about 1600 ^{4}He atoms or 4300 ^{3}He atoms from the droplets. Droplet size measurements before and after pick-up of SF_6 molecules by droplets consisting of 10^4 atoms reveal that approximately 600 atoms are evaporated for each captured molecule [72]. Thus these losses set a limit of about 1000 atoms on the minimum size of the, droplets which may be used. If the decrease of the droplet size upon pick-up can be neglected, that is, in the approximation of the constant pick-up cross section, the probability for pick-up of k particles is given by a Poisson distribution, where z is the average number of collisions which lead to capture of the particles by the droplet [95].

$$P_k(z) = \frac{(z)^k}{k!}\exp(-z) \qquad \textbf{(2.1)}$$

Owing to the superfluid state of the droplets, the k embedded species are free to move within the droplet and within a short time (presumably $\tau \approx 10^{-8}$ - 10^{-10} s) coagulate to form a single large complex or in some cases several smaller complexes [94]. It is illustrated the Poisson dependence of the depletion signal on the gas pressure in the pick-up cell, as measured for absorption bands corresponding to different number of

molecules in the $(molecule)_k$ complex. Solid curves are fits according to Equation (2.1) with a pick-up.

2.5.3. An example for the apparatus

The experimental setup for laser evaporation combined with helium nanodroplets has been tested in different machines using various lasers. Fig 2.3 gives an overview of the arrangement for doping and the different detectors used in experiments although not all the components shown in Fig. 2.3. have been combined in that order in a fixed apparatus.

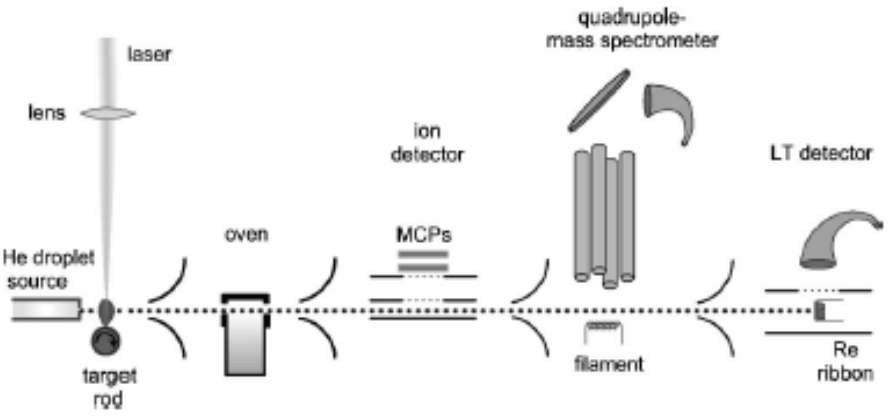

Figure 2.3: Experimental setup for doping metal ions comprised of a series of differentially pumped vacuum chambers

The molecular beam machine for generation of helium droplets has been used mainly for spectroscopic studies and is described in detail elsewhere. In short, helium gas (stagnation pressure P_0: 30–100 bar) expands through a cold (temperature T_0: 15–26 K) nozzle 5 μm in diameter. The droplet size can be varied by changing the expansion conditions (T_0, P_0). Behind the first skimmer (diameter: 400 mm, distance: 20 mm) is an oven that provides the vapor for pickup of the chromophores in a separate vacuum chamber. The cylindrical oven with 3 mm entrance and exit orifices is heated via radiation from a coaxial heater with tantalum coils. The oven was filled with sodium, for which we precisely know the doping conditions from spectroscopic measurements, i.e., the average number of sodium atoms per droplet. Further downstream under ultra high vacuum, (UHV) conditions several detectors have been used

1- A time of flight arrangement in which after pulsed extraction and a field free region ions can be mass analyzed by means of time correlated detection in a multichannel plate detector.

2- A quadrupole mass spectrometer in which neutral species are ionized by electron bombardment.

3- A Langmuir–Taylor surface ionization detector which can accurately measure the number of alkali and alkaline earth doped helium droplets [9].

The setup for doping the droplets by means of laser evaporation was installed directly in the droplet source chamber. Apart from the fact that in this way a doped helium droplet beam can be produced with only one vacuum chamber, there is another crucial reason choosing this option. In order to carry dopants, the helium droplets have to dissipate the kinetic energy upon impact by evaporation of helium atoms. The total energy a droplet of 10 000 helium atoms can dissipate by complete evaporation is 6 eV. Since the atoms from laser plasma have large kinetic energies, the probability of ejected particles being trapped in a droplet is low. Having the laser-evaporated atoms directly in front of the nozzle allows two extra processes: on one hand the ejected atoms with high kinetic energy can be ‘‘precooled’’ during scattering processes with the high density of the outer beam of helium atoms. This major part of the expanded helium is skimmed upon entry into the second chamber in order to establish the good vacuum conditions required downstream. On the other hand, the laser evaporated material can directly serve as a seed and enhance condensation of droplets. The measured cluster size distributions presented later indicate that the latter process appears to be important.

The dopant material is evaporated from a target rod which is oriented perpendicularly with respect to the droplet beam. No housing or shielding was installed. The rod carries out rotational and translational motion in order to evenly spread ablation over the rod of 3-5 mm in diameter. The position (distance from the nozzle and distance from the droplet beam) can be varied during operation. The optimal position was found to be 6 mm below the beam axis and 10 mm away from the nozzle, although there is no substantial dependence of the measured intensities on the exact position. For the ablation a frequency doubled Nd:YAG laser (λ=532 nm) and alternatively an excimer laser

(λ=308 nm) was focused (f=300 mm) onto the target material.The energy per pulse was of the order of 20 mJ. The optimum energy is material dependent and not very crucial. Repetition rates up to 50 Hz have been used, limited only by the lasers available [18].

2.6. Theoretical Studies

A great variety of theoretical models have been used to compute the potential energy curves of the alkali ion-rare gas pairs [96]. Extensive ab initio calculations, including correlation energy, using a correlated electron pair approximation (CEPA) by Hariharan and Staemmler [53] are available for the $LiHe^+$ ion. For the heavy alkali-ion systems, due to the great number of electrons, only more approximate calculations are feasible.

An electron gas Drude model by Gordon and Kim [97] has given promising results for all the alkali-rare gas pairs. This method uses a statistical procedure to calculate the repulsive part of the potential and then adds an empirical potential to include the dispersion and induction forces. A slightly modified approach was suggested by Gianturco [96]. He directly corrected the leading induction term at short distances by defining an effective polarization potential

$$V_{pol}(r) = -(\alpha/2r^4)w(r) \qquad \textbf{(2.2)}$$

with α the polarizability of the rare gas and w(r) a cut-off function. Two basic assumptions of that model are: (i) the overlap of the charge densities is negligible, and (ii) the electrostatic picture of a point charge interacting with an induced dipole, which is valid at long-range distances would hold at intermediate distances [64].

The close agreement of the present experimental results with those of Skullerud [50] as well as the MCS reproduction of all three transport coefficients using the interaction potential proposed by Larsen [65] over the entire range of E/N (electric field to neutral-particle number density ratio) studied not only provides confirmation of their transport coefficient values, but also lends strong support for their proposed interaction potential. In comparison, the more recent potentials of Ahlrichs and of Koutselos [66,49] reproduce the experimental data quite as well. As a benchmark the MCS calculations have also provided evidence of the accuracy of the Kramers-Moyal expansion method in calculating the transport coefficients.

The calculation was improved by Senff and Burton [54], by using a more complete basis set and including basis set superposition error corrections in all results. Larsen [65] summarized the work to date, and compared the experimental data available with those calculated from the potential of Senff and Burton.

Two quite reasonable potential models are presently available 15 years ago for the alkali ion–noble gas systems: the 'Tang–Toennies model' [55], and the 'Koutselos–Mason–Viehland model' [98, 99].

The accuracy of ab initio methods has been improved tremendously in recent years since the first comparisons between derived potentials obtained from ion beam studies[100] and initial ion mobility studies [101].

The $NaRg^+$ complexes have been studied by Ahmadi [16] and Soldan [17] and their ab-initio results appear to be very reliable. Breckenridge and his group have performed experimental and theoretical studies on numerous complexes of rare gases and metal or metal ions. For instance, one of the most recent studies investigates the effects of M^+ permanent quadrupole moments on the metal ion-rare gas bonding [102].

Experimental and theoretical studies of the bond between an excited state of magnesium and rare gases have been reported by Breckenridge [103]. Calculations for $MgNe^+_n$ complexes with n=1, 2, 3, 4 have been performed with the magnesium monocation in the ground state [22]. Magnesium-Helium complexes where the oxidation state of magnesium was varied between 0 and +2, have been studied theoretically by Leung [104]. The mobility of potassium and sodium ions in helium has recently been calculated by Moszynski [105,106] using ab-initio quantum chemical methods to obtain the interaction potential followed by a numerical solution of the Boltzmann equation. The experimental mobilities are compared with values calculated from a new and accurate ab initio potential [50,107]. Diffusion and interaction potentials for K^+ ions in the noble gases calculated by using ab initio methods using a modified Tang–Toennies-type potential model with hyperpolarizabilities included and a generalized Born–Mayer-type repulsive term.

As an example to the present works; microsolvation of Li^+ in bosonic He clusters is studied in the view of many body effects on the structure of the small aggregates. [108].

The $LiHe^+_n$, the $NaHe^+_n$, and the $MgHe^+_n$ complexes with n=1, 2, 3, 4 were studied using MP2 (Moller-Plesset of second order) method with 6-311+G (3df, 3pd) basis. Vibrational frequencies were calculated for Na and Mg with n=1, 2 for Li with n=1, 2, 3. In addition, vibrational frequencies for the $MgHe_3^+$ complexes were calculated at MP2 level [69].

Interatomic potential energy curves were presented by Soldan for the Na^+- Rg, Li^+-Rg and K^+-Rg (Rg=He, Ne and Ar) cationic complexes [102,109,110]. CCSD(T) calculations were employed with the pv5z basis to calculate interatomic potentials over a wide range of separations, as demanded by the transport property calculations. Both the calculated spectroscopic data and transport data showed that the ab initio potentials are better than the previous theoretical results. The excellent agreement with the model potentials of Skullerud [99] which were based on a simple model potential with parameters fitted to accurate mobility data, and the ab-initio potentials indicate that truly reliable potentials are available even for the KHe^+ species.

3. METHODS

3.1. Programs and technical supports used in calculations:

Gaussian 2003 [111] is a powerful computational tool and designed to work efficiently given a variety of computer configurations from a PC to a supercomputer. Source code and also binary codes are available for almost all operating systems. Gaussian 2003 does several types of calculations, including single-point energy calculation, geometry optimization, transition state location, vibrational frequency calculation, thermochemical analysis, excited states calculation, including solvent effect, and calculaton of electrostatic potential-derived charges and polarizabilities. An extremely wide variety of *ab initio* and semi-empirical methods are supported. All ab-initio, DFT calculations are performed by using this software.

A typical gaussian input, used in this work likes;

%mem=360MW	Link 0 section
%nproc=4	Number of processors used by the job
%rwf=245mw	Memory disk storage determined
#maxdisk=245mw	Route section (# lines)
# CCSD(T)=full cc-pv5z counterpoise=2 scan test t	
sodium-helium + potential	Title section
1 1 1 1 0 1	Molecule specification
Na 0. 0. 0. 1	
He 1 r 2	
r 2.3 S 8 0.1	

- Link 0 Commands: Locate and name scratch files.
- Route section (# lines): Specify desired calculation type, model chemistry and other options
- Title section: Brief description of the calculation.
- Molecule specification: Specify molecular system to be studied.

In this job, the route section consists of two lines. The molecule specification section begins with a line giving the charge and spin multiplicity for the molecule. The charge and spin multiplicity line is followed by lines describing the location of each atom in the molecule, since the molecule is formed by two atoms, it is lineer and no coordinate is given. The potential energy between Na^+ and He is calculated by using CCSD(T) method and pv5z basis at 8 points of internuclear separation r, started from 2.3 Å and incremented by 0.1 Å. The theoretical study of molecular interactions under the supermolecular approach with finite basis sets centered at the atomic positions originates the so-called Basis Set Superposition Error (BSSE). Within the LCAO-MO approach, each fragment can be expanded to some extent in the basis set of the partner. Thus, BSSE is the unphysical effect due to the improvement of the quantum mechanical description of the fragments within the supermolecule. It has been recognised for long time that this effect results in an increase of the interaction energy.

The most widely used method to handle BSSE has been the *a posteriori* Counterpoise method. The counterpoise procedure has been used mainly to obtain corrected interaction energies.

All our calculations has been carried out on the linux clusters at the Institute of Informatics.

A public-open software called Level [112] is used for calculating the vibrational bound states of the potential curves calculated in this work. This software, in general, calculates eigenvalues, expectation values, Franck-Condon factors and other matrix elements of arbitrary radial or effective one-dimensional potentials for diatomic molecules.

3.2. Methods and basis sets used in calculations

The list of the methods that we used throughout the calculations are given below.

- MP2 (Moller-Plesset of second order) :Only the description of the valence electrons
- MP2=full : The MP2 applied to all electrons of the system
- MP4=full : Runs over all single, double, triple and quadruple excitations
- QCISD(T): Requests a Quadratic CI calculation, including single and double substitutions with a triples contribution to the energy added.
- CCSD(T): Coupled cluster calculations, using double substitutions from the Hartree-Fock, both single and double substitutions for CCSD include triple excitations non-iteratively
- B3LYP: Becke Three Parameter Hybrid Functionals

3.2.1. Post -HF Methods-Consideration of the Electron Correlation

It is recognized that refinement of the HF procedure proceeds in two distinct directions. One is extension of the basis set of basis functions used for expansion of the spin-orbitals. The other is the development of methods for taking account of the correlation of electrons that is neglected in the simplest, single-determinant HF treatment. The extension of the basis set would only lead, in the best case of an infinite basis, to the HF limit, which does not include all components of electron correlation. To account for these contributions, a wide variety of methods have been proposed and some are now widely used in practical applications. Ideally, a theoretical model taking electron correlation into consideration should be [130]

(1) Well defined, leading to a unique energy for any nuclear configuration and a continuos potential surface

(2) Size consistent, so that when applied to an ensemble of N isolated molecules, calculated energies should be additive, e.g. N = 2 then

$$E(AA) = 2\,E(A) \qquad \textbf{(3.1)}$$

If this condition is not satisfied, the theory is unlikely to give a good description of the relative energies of molecules of different sizes.

(3) It should be exact (equivalent to full CI) when applied to a two-electron system.

(4) It should be variational, so that the computed energy is an upper bound to the correct energy.

Few theories satisfy all these conditions, even for molecular ground states. HF theory, in its spin-unrestricted form (UHF) with an atom-centered set of basis functions, usually satisfies all four but takes no account of the correlation between electrons of opposite spin. Complete configuration interaction (full CI), within a given basis, would satisfy all conditions, but this is only practical for very small systems. This leads to two additional conditions:

(5) It should be accurate enough to give an adequate approximation to the full CI result.

(6) It should be efficient, so that computation with large basis sets is possible.

Current methods do not satisfy all these criteria and mostly compromised by introducing different approximations with varying degrees of success.

3.2.1.1 Møller-Plesset Perturbation Theory

The Møller- Plesset method [113], a different approach to electron correlation has become very popular in recent years. In this method, higher excitations are taken into account by a perturbation operator ($\underline{P}$) within the many body perturbation theory introduced by Rayleigh and Schrödinger. The HF problem is treated as the unperturbated wave function and the residual part of the Hamiltonian is treated as a perturbation:

$$\underline{H} = \underline{H}^{\circ} + \underline{P} \qquad \textbf{(3.2)}$$

The application of the perturbation theory is justified, if the contribution of electron correlation energy (the "perturbation“) is small. This is usually the case.

In the HF computations, the energy eigenvalues $E^{(0)}$ and eigenfunctions $\Psi^{(0)}$ are known from the solution of the unperturbated system with

$$\underline{H}^{\circ}\Psi^{(0)} = E^{(0)}\Psi^{(0)} \qquad \textbf{(3.3)}$$

If the perturbation is small, then $\Psi^{(0)}$ and $E^{(0)}$ lie close to the exact wave function, and the energy.

Assuming these two conditions, a generalized electronic Hamiltonian ($\underline{H}_\lambda$) can be defined as:

$$\underline{H}_\lambda = \underline{H}^{\circ} + \lambda \underline{P}. \qquad \textbf{(3.4)}$$

Expanding the wave function (Ψ_λ) and energy as a power series:

$$\Psi_\lambda = \Psi^{(0)} + \lambda^1\Psi^{(1)} + \lambda^2\Psi^{(2)} + \ldots \quad = \sum_{n=0}^{\infty} \lambda^n \Psi^{(n)} \qquad \textbf{(3.5)}$$

$$E_\lambda = E^{(0)} + \lambda^1 E^{(1)} + \lambda^2 E^{(2)} + \ldots \quad = \sum_{n=0}^{\infty} \lambda^n E^{(n)} \qquad \textbf{(3.6)}$$

where λ is an arbitrary parameter included to keep track of the orders of perturbation applied.

Ψ_λ and E_λ represent the exact or full CI (within a given basis set) ground state wave function and energy for a system described by the Hamiltonian, $\underline{H}_\lambda$. For $\lambda = 0$, $\underline{H}_\lambda$ equals the unperturbated operator $\underline{H}^{\circ}$.

The following eigenvalue equation now can be solved:

$$\underline{H}_\lambda \Psi_\lambda = E_\lambda \Psi_\lambda \qquad \textbf{(3.7)}$$

by substituting the wave function and energy as power series

$$\left(\underline{H}^{\circ} + \lambda \underline{P}\right)\left[\Psi^{(0)} + \lambda^1\Psi^{(1)} + \lambda^2\Psi^{(2)} + \ldots\right] = \left(E^{(0)} + \lambda^1 E^{(1)} + \lambda^2 E^{(2)} + \ldots\right)\left[\Psi^{(0)} + \lambda^1\Psi^{(1)} + \lambda^2\Psi^{(2)} + \ldots\right] \qquad \textbf{(3.8)}$$

expanding the products and collecting like terms of λ together and equating them. The resultant equation is as follows:

$$E^{(0)} = \left\langle \Psi^{(0)} \middle| \underline{H}^{\circ} \Psi^{(0)} \right\rangle, \quad E^{(1)} = \left\langle \Psi^{(0)} \middle| \underline{P} \Psi^{(0)} \right\rangle, \quad E^{(2)} = \left\langle \Psi^{(0)} \middle| \underline{P} \Psi^{(1)} \right\rangle \quad \text{...} \quad \textbf{(3.9)}$$

All resulting terms can be expressed in terms of $E^{(0)}$, $\Psi^{(0)}$ and the determinable term $\left\langle \Psi^{(0)} \middle| \underline{P} \Psi^{(0)} \right\rangle$. The unperturbated, ground state wave function and energy can be written in terms of the occupied, one-electron spin orbitals, Ψ^{b} where ε_i is the energy of any single spin orbital.

$$\Psi_0 = \Psi^{(0)} \text{ and } E_0 = E^{(0)} = \sum_{i \in \Psi^{b}} \varepsilon_i \qquad \textbf{(3.10)}$$

Møller and Plesset perturbation operator is written as:

$$\underline{H}_{\lambda} = \underline{H}^{\circ} + \lambda \underline{P} = \sum_i \underline{F}_i + \lambda \left[\sum_{i,\, j;\, i<j} \frac{1}{r_{ij}} - \frac{1}{2} \sum_i (\underline{J}_i - \underline{K}_i) \right] \qquad \textbf{(3.11]}$$

$E^{(0)}$ is the sum of the one-electron energies and therefore, only the sum $E^{(0)} + E^{(1)}$

$$E^{(0)} + E^{(1)} = \left\langle \Psi^{(0)} \middle| \underline{H}_{\lambda} \Psi^{(0)} \right\rangle \qquad \textbf{(3.12)}$$

represents the HF energy since $\Psi^{(0)}$ corresponds to the HF wave function.

To calculate $E^{(2)}$ the first order wave function $\Psi^{(1)}$ has to be known. This is given by:

$$\Psi^{(1)} = \sum_{s>0} (E_0 - E_s)^{-1} P_{s0} \Psi_s \qquad \textbf{(3.13)}$$

Ψ_s, is the sum of one-electron energies of those spin-orbitals which are occupied with the energy, E_s . P_{s0} are the matrix elements of the perturbation operator. It can be shown that P_{s0} does not become zero, if s corresponds to a determinant with double substitutions. Thus only double substitutions contribute to the first order wave function.

Due to the good cost (CPU time) to accuracy ratio, the power expansion is often truncated after the second order, known as MP2 level, for which the energy is:

$$E^{MP2} = E^{(0)} + E^{(1)} + E^{(2)} = E^{HF} + E^{(2)} \qquad \textbf{(3.14)}$$

The energy $E^{(2)}$ ($\Psi_k(\boldsymbol{x})$ are spin orbitals; where indices, i and j, correspond to the occupied spin orbitals, Ψ^b, and indices, r and s, correspond to the unoccupied spin orbitals, Ψ^u) is given by:

$$E^{(2)} = \sum_{\substack{i,j \in \Psi^b; \\ i<j}} \sum_{\substack{r,s \in \Psi^u; \\ r<s}} \frac{\iint \left(\left| \Psi_i^*(\boldsymbol{x}_1)\Psi_j^*(\boldsymbol{x}_2)\frac{1}{r_{12}}\Psi_r(\boldsymbol{x}_1)\Psi_s(\boldsymbol{x}_2) - \Psi_i^*(\boldsymbol{x}_1)\Psi_j^*(\boldsymbol{x}_2)\frac{1}{r_{12}}\Psi_s(\boldsymbol{x}_1)\Psi_r(\boldsymbol{x}_2) \right|^2 \right) d\boldsymbol{x}_1 d\boldsymbol{x}_2}{\varepsilon_i + \varepsilon_j + \varepsilon_r + \varepsilon_s} \qquad \textbf{(3.15)}$$

The third order energy, like MP2 only incorporates contributions from double substitutions [114,115]. Only at MP4 level, additional single, double, triple (MP4 SDT) and quadruple (MP4 SDTQ) substitutions are included [116,117]. The MPn method is a size-consistent, but not variational method. Electron correlation is not introduced in the first order (i.e. MP1 = SCF). Second order energy correction only involves doubly excited determinants coupling with the reference determinant. Third order energy correction only involves doubly excited determinants coupling with each other and the reference determinant. Fourth order energy correction involves doubly excited determinants coupling with the reference determinant as well as with singly, doubly, triply and quadruply excited determinants.

It is a drawback that MP series sometimes converges slowly, especially in systems where the effects of correlation are large. The MP4 method is a practical method but limited to relatively small systems. The MP2 method can be used extensively even for larger systems but, it must be used with reasonable basis sets (e.g. 6-31G* or better). MP3, MP4 and MP5 are more complicated and much more time-consuming compared to MP2. The conventional ab initio results show interesting convergence properties with

the level of theory used. The MP2 and MP4 energies are extremely similar. The MP3 interaction on the other hand produces a significantly shallower well. As expected the single determinant Hartree-Fock interaction did not posses an attractive well.

In this work MP2, MP2=full, MP4=full calculations are done. To save CPU time and disc space, MP computations are often carried out with a frozen core (FC) which indicates that correlation effects on the total energy of the inner-shell electrons are excluded from calculation. That is, only valence-shell electrons are considered in the electron-correlation computation. This procedure utilizes the fact that only valence electrons take part in chemical bond formation. In contrast to a frozen core computation, the calculations in which all electron correlations are included is called MPn full. MPn-full calculations have been carried out to understand the effects of the core electrons and to see the improvements in the potential energy curves.

3.2.1.2.Configuration Interaction(CI)

The starting problem is the same as for the HF method. The eigenfunction and eigenvalues of the Schrödinger equation within the Born Oppenheimer picture can be computed considering the electron correlations explicitly for many electron systems.

The neglect of one part of the correlated motion of electrons is a consequence of the approximation of the total wave function by a single-determinant within the HF theory. Therefore, an extension of the orbital space should result in an improvement and include electron correlation. This can be achieved using a linear combination of Slater determinants to describe the total wave function:

$$\Psi^{el} = a_0 \Psi_0^{SD} + a_1 \Psi_1^{SD} + \ldots = \sum_{k=0}^{L} a_k \Psi_k^{SD} \qquad \textbf{(3.16)}$$

(L = corresponds to a full- and L < to a limited CI calculation).

With the term configuration interaction, two different meanings can be associated. Mathematically, a "configuration" is understood to be a linear combination of Slater determinants built from spin orbitals. Chemically, it is a specification of the occupation of the orbitals, e.g. $(1s)^2$ $(2s)^1$,..etc. The configuration interaction is the mixing (interaction) of different electronic configurations (states). In this case, the CI method is

a special case of the more general method of the linear combination of Slater determinants.

The CI procedure represents a linear variation method leading to a general matrix eigenvalue problem:

$$Ha = \varepsilon Sa \qquad \textbf{(3.17)}$$

with the energy matrix H: $(H)_{ik} = \left\langle \Psi_i^{SD} \left| \underline{H}^{el} \Psi_k^{SD} \right\rangle \right.$ **(3.18)**

the overlap matrix S: $(S)_{ik} = \left\langle \Psi_i^{SD} \left| \Psi_k^{SD} \right\rangle \right.$ **(3.19)**

and the coefficient vector a as well as ε the eigenvalue matrix corresponding to the energy matrix H.

By definition, all Slater determinants are constructed from a set of orthonormal spin orbitals. Therefore:

$\left\langle \Psi_i^{SD} \left| \Psi_k^{SD} \right\rangle \right. = \delta_{ik}$ leading to S = 1 (= E, identity matrix). **(3.20)**

In this case, the above general matrix eigenvalue expression can be simplified to

Ha = εa.

In general, a finite linear combination of Slater determinants, which are constructed from HF-SCF orbitals using the unoccupied "virtual" orbitals, is employed. In the case of HF spin orbitals, $\Psi_0^{SD} = \Psi^{HF}$ represents the HF wave function (reference determinant) and $\Psi_1^{SD} + \Psi_2^{SD} + \ldots \Psi_L^{SD}$ are determinants in which occupied orbitals are substituted by virtual orbitals also obtained in the HF computation. Substituting a virtual orbital (j*) for an occupied orbital [118] in the HF reference determinant, the resultant determinant (Ψ_i^{j*}) is known "singly excited". If doubly-substituted configurations are included (k*,l*εi,j), the determinant (Ψ_{ij}^{k*1*}) is called "doubly excited". Following this convention, the overall wave function is expressed as:

$$\Psi^{el} = \Psi^{HF} + \sum_{i,j^*} a^{S}_{ij^*} \Psi_i^{j^*} + \sum_{i,j,k^*1^*} a^{D}_{ijk^*1^*} \Psi_{ij}^{k^*1^*} + \ldots \qquad \textbf{(3.21)}$$

By this procedure, the HF wave function will be mixed with linear combinations of excited states. The degree of mixing is regulated by the coefficients ($a^{S}_{ij^*}$ single substitutions, $a^{D}_{ijk^*1^*}$ double substitutions, ...)

Applying the HF method (Roothaan-Hall procedure), in which the spin-orbitals are approximated by a fixed basis functions,

$$f_p^B(\boldsymbol{r}) \; (p = 1,2,\ldots, \text{A with } 2A \geq N) \qquad \textbf{(3.22)}$$

to a system of N electrons, 2 A orthonormal, optimized spin orbitals (N occupied and 2A-N virtual spin-orbitals) will be generated. Thereby, the maximum number of "excited" determinants is limited by the basis set [119].

The special matrix eigenvalue problem of the CI method is a genuine eigenvalue problem, which can easily be solved by diagonalizing of H. In this procedure, only the coefficients, a_k, of the determinants, but not the coefficients, c_{ip}, of the basis functions will be optimized.

In practice, a CI computation starts with the optimization of the HF wave function. From that HF reference wave function, the excited states (with the same spin and space symmetry, the so- called configuration state functions, CSF) are constructed. Subsequent to the HF calculation, the eigenvectors a and the corresponding eigenvalues are determined by diagonalizing of H. With the help of the Slater-Condon rules, the matrix elements of H

$$(H)_{ik} = \left\langle \Psi_i^{SD} \left| \underline{\underline{H}}^{el} \Psi_k^{SD} \right\rangle \right. \qquad \textbf{(3.18)}$$

are analyzed. The determination of the matrix elements, H, takes about 99% of the CPU time, whereas the solution of the eigenvalue problem requires only 1% of the CPU time.

In general, CI is not the most practical method for the calculation of correlation energy, because full CI is not possible. Therefore, convergence of the CI expansion is slow, and

the integral transformation, time-consuming. In practice, only a limited (or truncated) configuration interaction has been used extensively. If all doubly-substituted configurations from the HF reference determinant are included, the method is called CID. If single substitutions are added, it becomes CISD. The energy, calculated as the expectation value of the electronic Hamiltonian for CISD is:

$$E_{CISD}^{el} = \frac{\left\langle \Psi^{CISD} \middle| \underline{\underline{H}} \Psi^{CISD} \right\rangle}{\left\langle \Psi^{CISD} \middle| \Psi^{CISD} \right\rangle} = E_{HF}^{el} + \sum_{i<jk^*<1^*} \sum a_{ijk^*1^*}^{D} \left[\left(ij|k^*1^* \right) - \left(ik^* \middle| j1^* \right) \right] \quad \textbf{(3.23)}$$

More generally, the name given to a particular type of configuration interaction calculation is depending on the degree of truncation employed: S = single, D = double, T = triple, Q = quadruple. Any combination can be used. For example CISDQ means a CI computation including singlets, doublets and quadruplets. Usually, double substitutions (D), followed by the less important quadruple substitutions (Q) give the largest contributions to the correlation energy [121].

All CI calculations are variational, but fail to satisfy the important size-consistency condition except for the full CI which is size-consistent. In applications where a large range of molecules is considered, size-consistency is generally regarded as being more important than fulfilling the variational criterion. CISD results are therefore usually modified by a simple correction introduced by Langhoff and Davidson, which makes the energies approximately (not exactly!) size-consistent, but no longer variational [122]

$$\Delta E^{correction} = (1 - a_0^2) \Delta E^{CISD} \quad \textbf{(3.24)}$$

where ΔE^{CISD} is the correlation energy at CISD level and a_0 is the expansion coefficient of the HF wave function in the linear combination of the Slater determinants being used for the CISD wave function. However, this Davidson correction fails to give the correct answer for a two-electron system. Here, CISD is equivalent to full CI, where this correction is not needed. The CISD method also omits effects of triple substitutions, which are known to be important [123]. The quadratic configuration interaction method [124] was developed to ensure size consistency in the resulting total energy. The conventional equations of (linear) configuration interaction theory are modified by

introducing new terms, which are quadratic in the configuration coefficients. It is applied in the truncated configuration space of single and double substitutions. The method, termed QCISD, leads to a tractable set of quadratic equations. QCISD also accounts for some correlation effects to infinite order. Furthermore, the quadratic configuration procedure (QCISD) can be regarded as a simplified approximation of CCSD. The next level, QCISDT, which incorporates triple substitutions, is impractical at present.

A useful approximation for triple substitutions, is to treat them as a perturbation of the solution already obtained at the singles-doubles level, resulting in the method denoted by QCISD (T) which was used in this study. It is the CI method giving a perturbative estimate of the effects of triple excitations. It is noticeably better than QCISD, but also more expensive.

Due to long CPU time and immense hardware requirements, CI methods are still limited to relatively small systems like ours.

3.2.1.3. Coupled Cluster Theory

Pair theory is a physically inspired approach to incorporating electron correlation. According to Pauli's principle, no more than two electrons are allowed to come close to each other, resulting in the idea that pair correlation must represent the major part of electron correlation. Pair theory is a particular type of coupled cluster theory. This theory uses a wave function which can be generally written as a sum of

$$\Psi = \Psi_0^{SD} + \Psi_1^{SD} + \Psi_2^{SD} + \Psi_3^{SD} + \ldots \qquad \textbf{(3.25)}$$

where Ψ_2^{SD} describes the correlation of two, Ψ_3^{SD} of three electrons etc. This expansion is finite and the series can be calculated recursively from Ψ_0^{SD}. When the expansion is truncated after Ψ_2^{SD}, this is referred to as pair theory. Pair theory can be split into several categories, among which are IEPA (independent electron-pair approximation) and CEPA (coupled electron-pair approximation), which is also known as CCD (coupled cluster double excitation).

First introduced in nuclear physics [125], this approach was adapted for the molecular problem by Cizek [126]. It satisfies the size-consistency condition, but like the MP method, not variational. It offers a better approximation than perturbation theory, if the correlation correction is large (i.e. large perturbation means that the MP method becomes unreliable).

Starting with the HF reference wave function (in the ground state), the CC procedure is based on the exponential ansatz :

$$\Psi^{el} = e^{\underline{T}}\Psi_{HF}^{SD} = \sum_{b=1}^{\infty}\frac{1}{b!}\underline{T}^{b}\Psi_{HF}^{SD} \qquad \textbf{(3.26)}$$

where $\underline{T}$ is the cluster operator of a N electron-containing system:

$$\underline{T} = \sum_{i=1}^{N}\underline{T}_i \qquad \textbf{(3.27)}$$

and the individual members are defined as follows:

$$\underline{T}_1 = \sum_{i,r} a_i^r \underline{t}_i^r, \quad \underline{T}_2 = \sum_{i<j}\sum_{r<s} a_{ij}^{rs}\underline{t}_{ij}^{rs} = \frac{1}{4}\sum_{i,j,r,s} a_{ij}^{rs}\underline{t}_{ij}^{rs}, \qquad \textbf{(3.28)}$$

$\underline{T}_3 =$ analogous to triple substitutions.

In these expressions, the indices, i, j, k, l,.., characterize occupied spin-orbitals and r, s, t, u, ... virtual spin-orbitals. Introducing substitution operators, e.g. for a double substitutions ($\underline{t}_{ij}^{rs}$), which are defined by their influence on the HF wave function ($\Psi_{HF}^{SD} = \Psi_0$ if the HF determinant is the reference):

$$\underline{t}_{ij}^{rs}\Psi_0 = \Psi_{ij}^{rs} \qquad \textbf{(3.29)}$$

Here, Ψ_{ij}^{rs} corresponds to a "doubly-excited" single-determinant function in which the spin-orbital, i (j), is substituted by the virtual spin-orbital, r(s). The operator, $\underline{t}_{ij}^{rs}$, is antisymmetric in both (ij) and (rs).

In a CC calculation, the a-coefficients, which control the degree of orbital substitution, have to be determined. From these coefficients, the wave function and the energies can be derived. If the wave function of the Schrödinger equation is substituted for the above exponential expansion, equations which allow the determination of the coefficients are derived. However, the derivation is non-trivial and the resultant equations are both complex and non-linear.

In practice, the CCD method is most commonly applied. This method uses a wave function containing all possible double excitations [127]. This is mathematically achieved by approximating the cluster operator as:

$$\underline{T} \approx \underline{T}_2 \tag{3.30}$$

so that the wave function can be expressed as

$$\begin{aligned}\Psi_{CCD}^{el} &= e^{\underline{T}_2}\Psi_0 = (1+\underline{T}_2+\frac{1}{2}\underline{T}_2{}^2+\ldots)\Psi_0 \\ &= \Psi_0 + \frac{1}{4}\sum_{\substack{i,j,\\r,s}} a_{ij}^{rs}\,\underline{t}_{ij}^{rs}\Psi_0 + \frac{1}{32}\sum_{\substack{i,j,\\r,s}}\sum_{\substack{k,l,\\t,u}} a_{ij}^{rs}a_{kl}^{tu}\,\underline{t}_{ij}^{rs}\,\underline{t}_{kl}^{tu}\Psi_0 + \ldots\ .\end{aligned} \tag{3.31}$$

The product of the operators, $\underline{t}_{ij}^{rs}\,\underline{t}_{kl}^{tu}$, is treated as zero, if any of the eight indices are identical. If not, it leads to a quadruple substitution and becomes:

$$\Psi_{CCD}^{el} = \Psi_0 + \frac{1}{4}\sum_{\substack{i,j,\\r,s}} a_{ij}^{rs}\Psi_{ij}^{rs} + \frac{1}{32}\sum_{\substack{i,j,k,l,\\r,s\ t,u}}\sum a_{ij}^{rs}a_{kl}^{tu}\Psi_{ijkl}^{rstu} + \ldots\ . \tag{3.32}$$

The equations for the a-coefficients are obtained by projection of Ψ_{CCD} :

$$\underline{H}^{el}\Psi_{CCD} = E\Psi_{CCD} \quad \Leftrightarrow \quad \left(\underline{H}^{el} - E\right)\Psi_{CCD} = 0 \tag{3.33}$$

onto the function Ψ_0 and Ψ_{ij}^{rs}

$$\left\langle \Psi_0 \left| \left(\underline{H}^{el} - E \right) \Psi_{CCD} \right\rangle = 0 \right.$$

$$\left\langle \Psi_{ij}^{rs} \left| \left(\underline{H}^{el} - E \right) \Psi_{CCD} \right\rangle = 0 \right. \qquad \text{and finally} \qquad \textbf{(3.34)}$$

$$E = E_{HF} + \frac{1}{4} \sum_{i,j,r,s} \left\{ \int\int \Psi_i^*(\boldsymbol{x}_1) \Psi_j^*(\boldsymbol{x}_2) \frac{1}{r_{12}} \left[\Psi_r(\boldsymbol{x}_1) \Psi_s(\boldsymbol{x}_2) - \Psi_s(\boldsymbol{x}_1) \Psi_r(\boldsymbol{x}_2) \right] d\boldsymbol{x}_1 d\boldsymbol{x}_2 \right\} a_{ij}^{rs}$$

(3.35)

These equations are sufficient to determine the energy, E, and the unknown coefficients. Due to the quadratic term, $1/2 \cdot \underline{T}_2^{\,2}$, this system contains coupled, non-linear equations which can be solved iteratively. Neglecting this quadratic term leads to an approximation known as the linear CCD method (LCCD), or CEPA, according to the degree of approximation applied to the quadratic terms. The coupled cluster method is rapidly becoming a more important technique in computational chemistry. The CCSD [128] (coupled cluster including single and double substitutions) has been now extensively compared with CI for energies, equilibrium structures and infrared intensities in a variety of molecules. Results obtained indicate the superiority of CCSD over the CISD method. It is assumed that size consistency plays an important rule. Like CISD, the CCD and CCSD methods do not adequately account for triple substitutions. Some approximate treatments, which include triple terms have been introduced (CCSD(T)) which is the case used in this work, means iterative inclusion of triple excitations or higher is extremely expensive and restricted to very small systems [129,130]. CCSD(T)= CCSD+ non-iterative perturbative triples correction using CCSD amplitudes is the method used in this work.

3.2.2.Comparison of the Ab Initio Methods and Limitations

Hartree Fock theory is very useful for providing initial, first-level predictions for many molecular systems. However, the restricted HF theory has some basic deficiencies. It is insufficient for an accurate description of the energetics of reactions and bond dissociations, such as the dissociation of the H_2 molecule:

$$H^+ + H^- \quad \xleftarrow{RHF} \quad H-H \quad \xrightarrow{UHF,CISD} \quad H\cdot + H\cdot$$

A "dissociation catastrophe" occurs because the separated, one-electron hydrogen atoms cannot be described using doubly occupied orbitals. This means H_2 tends to dissociate into H^+ and H^-, which can be described by a doubly occupied orbital on H^- (closed shell). This problem does not occur in the UHF procedure, however, UHF does not give pure spin states

Generally speaking, the HF method is reasonably good at calculating the structures and vibrational frequencies of stable molecules. An additional inaccuracy stems from the neglect of the electron correlation arising from the interaction of electrons with antiparallel spin. Thus in HF, all computations of main group compounds result in bond distances that are too short, since antibonding states are not considered.

A variety of theoretical methods have been developed to attempt to account for electron correlation. To be satisfactory technique, the post-HF methods should ideally have six features.

Mφller- Plesset perturbation theory treats the correlation part of the Hamiltonian as a perturbation of the HF part and truncates the energy expansion at some order. This method is size-consistent at any order, but not variational. Moreover, MPn results can oscillate with the order of perturbation applied. An example from literature is the ab initio study on CrF_6. In this case, the total energy of both isomers (O_h and D_{3h}) "oscillate", depending on the order n of the applied MPn (n =1, 2, 3, 4) perturbation series. The O_h isomer is energetically favored by 18 (MP2) and 44 (MP4) kcal mol^1, whereas the D_{3h} isomer is more stable by 16 kcal mol, when the perturbation is truncated after the third order (MP3). The principal deficiency is that MPn series sometimes converge slowly and might become unreliable, when a large amount of electron correlation has to be considered.

The CI methods do not really represent an alternative to the MP method as a full CI is not feasible for most molecules. Limited CI methods (such as CID or CISD) have been used extensively. These methods are variational, but not size-consistent, which is, for many applications, a disadvantage, since it is generally more important being size-consistent than obeying the variation principle.

Alternative methods are CC and QCI, as well as the DFT (especially for larger systems). The CC method satisfies the size-consistency condition, but does not have the variational property. Further, it offers a better approximation than perturbation theory, if the correlation energy correction is large. For a two-electron system, it is equivalent to CID. Comparing the MP with the CCD method in terms of mathematical construction (and thereby in terms of energies), it can be shown that the CCD expansion is equivalent in λ to third order (MP3). In fourth order, the energy is equivalent to the MP fourth order energy, in the limited space of double and quadruple substitutions (MP4(DQ), rather than the full energy to fourth order, which would be the energy at MP4(SDTQ) level. The QCI methods are, in a sense, intermediate between CI and CC theory. The idea is to modify the CI equations in a simple manner, so as to restore size-consistency, but the loss of variational character. This requires additional terms, which are quadratic in the general substitution operators and leads to a treatment that is somewhat simpler than CC methods, at least for higher substitutions.

Within the HF-SCF procedure, the spin-orbital coefficients (c_{ip}) are optimized, whereas in a CI calculation the Slater determinant coefficients (a_k) are variationally optimized, while the spin orbital coefficients from which the Slater determinants are constructed, remain unchanged.

Unfortunately, these precise calculations are limited to very small systems and require considerable care in the selection of the basis set and especially, the active space. They should not be considered for routine use.

Although the approximate density functional theory does not strictly belong to ab initio methods, it has been employed successfully to obtain thermodynamic data, molecular structures, force fields and frequencies and is particularly useful for large systems, e.g. systems with transition metals. Here, correlation effects are included at a much lower cost. DFT already contains the necessary exchange-correlation terms and for the wave function no additional improvements are needed (beside the improvement of the basis set). This is in contrast to the HF method, where the approximation lies in the inadequate description of the wave function. In all post-HF methods (CI, CC, MPn ...), the wave

function is successively improved. The complexity of the approximate Ψ determines the level of theory [131].

3.2.3. A hybrid DFT method; B3LYP

The use of density functional theory (DFT) in the ab initio calculation of molecular properties has recently increased dramatically [132]. This can be attributed to

1) the development of new and more accurate density functionals,

2) the increasing versatility, efficiency, and availability of DFT codes, and, most

importantly,

3) the superior ratio of accuracy to effort exhibited by DFT computations relative to other ab initio methodologies.

Becke Three Parameter Hybrid Functionals is the method used in calculations. These functionals have the form devised by Becke in 1993 [133]:

$$A.E_X^{Slater}+(1-A).E_X^{HF}+B.\Delta E_X^{Becke}+E_C^{VWN}+C.\Delta E_C^{non\text{-}local} \quad \textbf{(3.36)}$$

where A, B, and C are the constants determined by Becke via fitting to the G1 molecule set.

The Becke3LYP functional [134,135] is a hybrid of several components, whose relative weights are chosen by reference to experimental thermochemical data. The accuracies of such hybrid functionals in predicting molecular geometries and vibrational frequencies have not yet been thoroughly characterized.

The popular B3LYP hybrid method, with 20% Hartree–Fock exchange, still systematically underestimates barrier heights [136], but raising the fraction of Hartree–Fock exchange usually deteriorated the quality of the prediction of the theory for other quantities more rapidly than it increased the quality of barrier height predictions. B3LYP calculations have been carried out to compare the DFT potential curves with the curves we obtained by using the post-HF methods.

3.2.4. Basis sets

cc-pvXZ(X=d,t,Q,5) basis sets which are Dunning's correlation consistent basis sets [137-139] (double, triple, quadruple, quintuple-zeta and sextuple-zeta, respectively) are used generally. These basis sets have had redundant functions removed and have been rotated in order to increase computational efficiency.

These basis sets are referred to as correlation consistent (or *cc*) and are designed such that a base set of sp functions is combined with correlation functions. These latter functions are chosen such that all functions in a given set lead to a similar lowering of the atomic correlation energy (calculated by CISD). The smallest member of this series and thus often the starting point for correlated calculations is the correlation consistent polarized double zeta basis set designated "cc-pVDZ".

Augmented functions, shown by aug, are diffuse functions for combination with the basis sets cc-pVXZ, cc-pV(X+d)Z, cc-pwCVXZ or cc-pV(X+d)Z; available for H, He, B-Ne, Al-Ar with X = D-6 and Ga-Kr with X = D-5.

They recover a large fraction of the correlation energy. Provide systematic improvements that converge toward the complete basis set limit. Consistently reduce errors at both the HF and correlated levels with each step up in quality.

The disadvantage is the number of basis functions doubles with each increase in quality.

Another basis set used for KHe^+ in calculations, is the Pople type basis called 6-31g**= 6-31G(d',p'), which is Split Valence + Polarization Basis set. Diffuse functions shown by * means, s-, p-, and d-functions with small exponents are usually added for specific purposes [140]. In addition, for CCSD(T) calculations, 6-311+G(3df, 3pd) [141] basis set that is the more advanced than 6-31g**, is used for KHe^+.

4. RESULTS AND DISCUSSIONS

4.1. Moller Plessed (MP) Calculations

In the first part of our calculations, the potential energy curve for MHe^+ (M=Li, Na, K) complexes are generated by using MP2 and MP2 (full) methods. For $LiHe^+$ and $NaHe^+$ complexes, cc-pv**X**z where X=d, t, Q, 5 basis sets are employed. For KHe^+, the cc-pv**X**z basis sets are not defined internally in Gaussian 2003 instead 6-31g** and 6-311+g (3df,3pd) basis set is used. For each potential energy curve, at approximately 60 internuclear separations, most of them around minimum, potential energy is calculated by subtracting BSSE (Basis Set Superposition Error) corrected energies of the fragments namely M^+ and He from the total energy of the supermolecule namely MHe^+ as follows:

$$V(R) = E(MHe^+)_R - E(M^+) - E(He) \qquad \textbf{(4.1)}$$

All the energies presented in this study are ZPE (zero point energy) corrected energies.

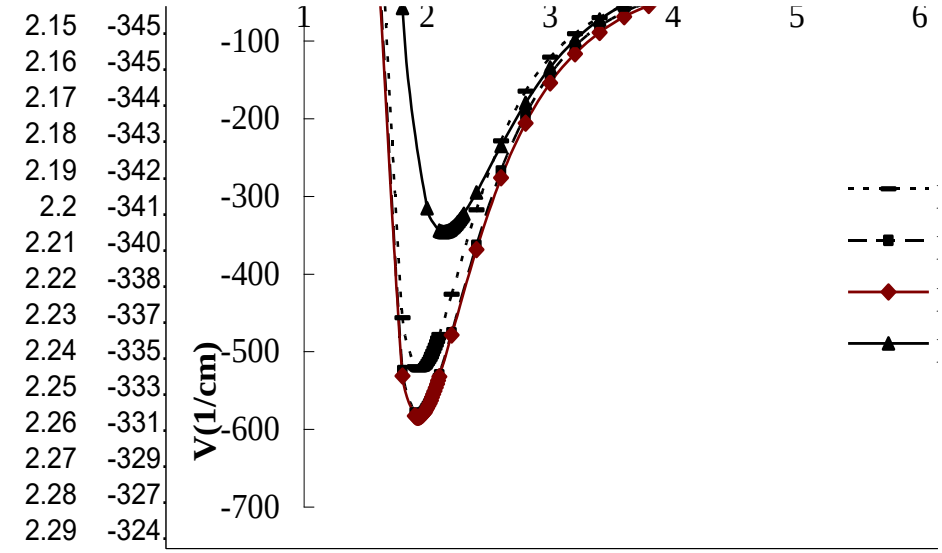

2.15	-345.				
2.16	-345.				
2.17	-344.				
2.18	-343.				
2.19	-342.				
2.2	-341.				
2.21	-340.				
2.22	-338.				
2.23	-337.				
2.24	-335.				
2.25	-333.				
2.26	-331.				
2.27	-329.				
2.28	-327.				
2.29	-324.				
2.3	-322.479	2.2	-426.282	-476.014	-478.748
2.400	-295.271	2.4	-317.812	-363.098	-368.647
2.600	-234.920	2.6	-228.725	-267.601	-276.102
2.800	-179.596	2.8	-164.626	-195.362	-205.736
3.000	-134.105	3	-120.822	-143.350	-154.037
3.200	-98.677	3.2	-90.923	-106.810	-116.361
3.400	-72.155	3.4	-69.870	-81.246	-88.915

Figure 4.1: PEC of $LiHe^+$ obtained from MP2 method with cc-pvdz, pvtz, pvqz, pv5z basis sets.

In Figure 4.1 the potential energy curve (PEC) for $LiHe^+$ calculated by using MP2 method with different basis functions are presented. The improvement in the PEC especially near the potential minimum can be easily seen upon increase of basis set. The asympthotic behaviour of different curves are almost the same. R_{min} values are slightly shifted towards smaller R values. The basis set consistency is observed as expected and the results obtained from cc-pv5z basis calculations are slightly better than cc-pvqz basis calculations.

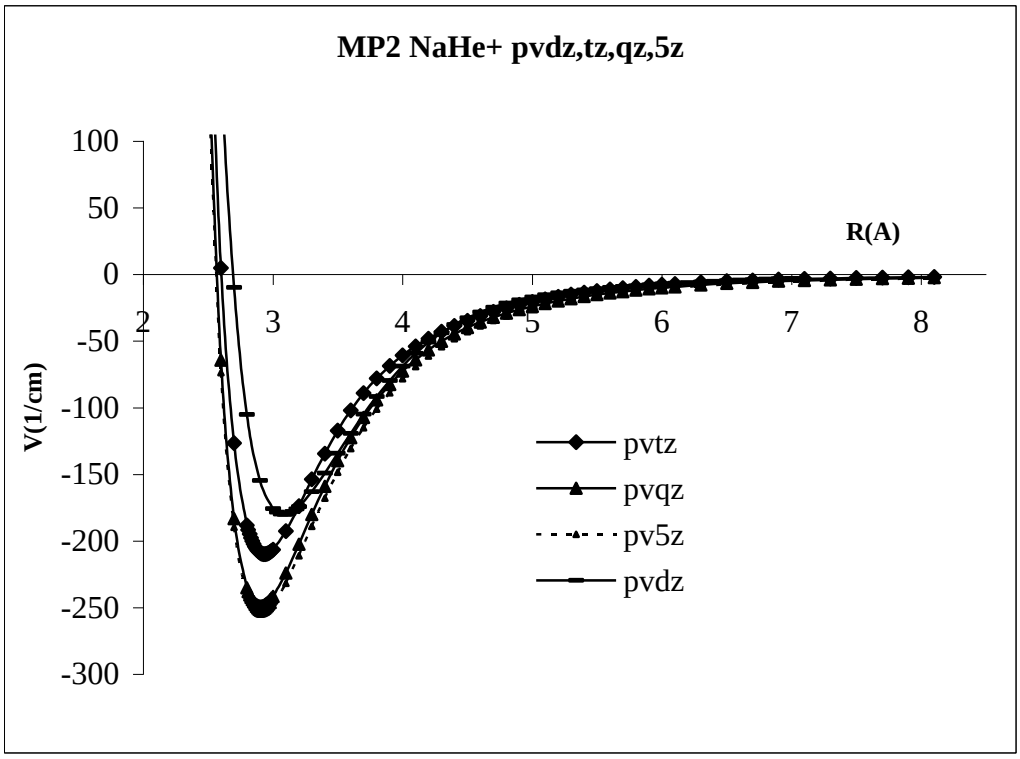

Figure 4.2: PEC of $NaHe^+$ obtained from MP2 method with cc-pvdz, pvtz, pvqz, pv5z basis sets.

In Figure 4.2, the potential energy curve (PEC) for $NaHe^+$ calculated by using MP2 method with different basis functions are presented. The improvement in the PEC with employing larger basis sets and the differences between them are more pronounced for this system. This is somewhat obvious result for the correlation consistent basis sets.

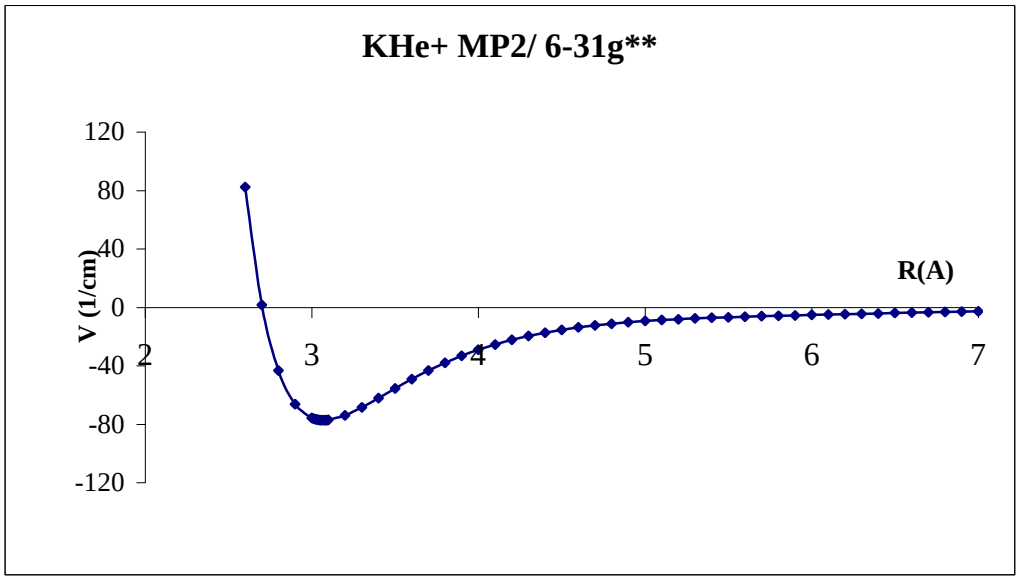

Figure 4.3: PEC of KHe^+ obtained from MP2 method with 6-31g** basis

In Figure 4.3, the PEC curve for KHe^+ is shown. The spectroscopic constants (R_e and D_e) given in Table 4.1. is totally incorrelated with the ones calculated by using different methods in the literature that will be given . This is actually expected since the basis set is not appropriate in describing the interactions in such systems whre there are many electrons. It is obvious that for a better curve, correlation consistent basis sets with post-HF methods must be employed.

Table 4.1 : Dissociation energies and bond lengths for $LiHe^+$,$NaHe^+$ and KHe^+. MP2 results with different basis sets.

MP2		**De (in 1/cm)**	**Re (in Å)**
LiHe+	pvdz	345,932	2,14
	pvtz	523,713	1,94
	pvQz	581,467	1,93
	pv5z	584,662	1,93
	6-311+(3df, 3pd) (69)	566.11	1,945
NaHe+	Pvdz	180,092	2,59
	Pvtz	209,880	2,43
	pvQz	248,814	2,40
	pv5z	254,828	2,41
	6-311+(3df, 3pd) (69)	282,90	2,437
KHe+	6-31g**	77,29	3,07

In the Table 4.1 the dissociation energies and bond lengths for $LiHe^+$,$NaHe^+$ and KHe^+ obtained from MP2 calculations with different basis sets are given. The R_e values predicted by MP2 method are 1.945 Å and 2.437 Å for $LiHe^+$ and $NaHe^+$ respectively. We can compare our results with the ones in literature. The only MP2 result we find is in 6-311+ (3df, 3pd) basis for $LiHe^+$ and $NaHe^+$ systems and given by Sapse and coworkers [69]. Their results for R_e and D_e values are larger than our pv5z results and similat to our pvtz results. The D_e differences are bigger in $NaHe^+$. We can say that MP2 results overestimate the internuclear separation and underestimate the dissociation energies for these systems. The comparison of the results to different methods and to experimental methods will be done in the next sections.

The next method we employed is MP2 (full) which means not only the valance electrons but also the core electrons are included in the correlation calculations. With the same cc-pvXz basis sets, the PEC's obtained are plotted in the Figure 4.4, Figure 4.5, Figure 4.6 for $LiHe^+$, $NaHe^+$, KHe^+ respectively. For the larger basis set calculations the convergence of the R_e and D_e values towards the experimental or the best theoretical calculations available in the literature is noticable. The error gets larger as the size of the molecule increases. The separation of the curves around minimum can be better seen. The basis-set dependent improvement of the PEC's are also observed here. This discussion here excludes the PEC for KHe^+ in which there is no improvement observed with MP2 (full) method.

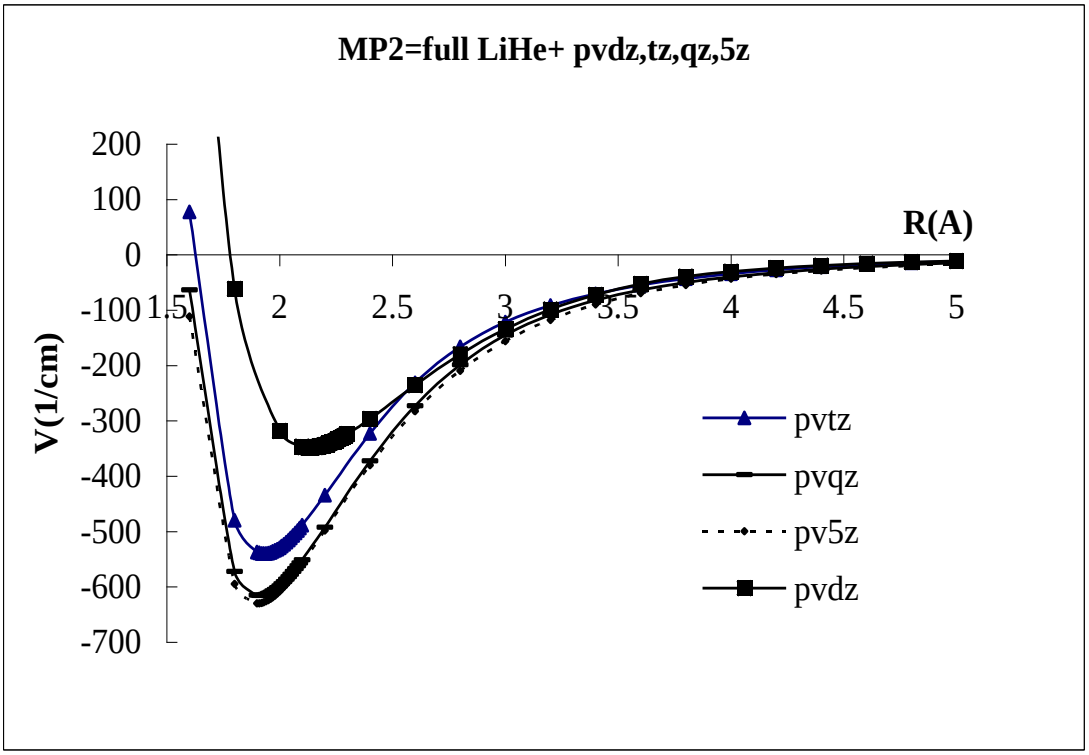

Figure 4.4: PEC of $LiHe^+$ obtained from MP2(full) method with cc-pvdz, pvtz, pvqz, pv5z basis sets.

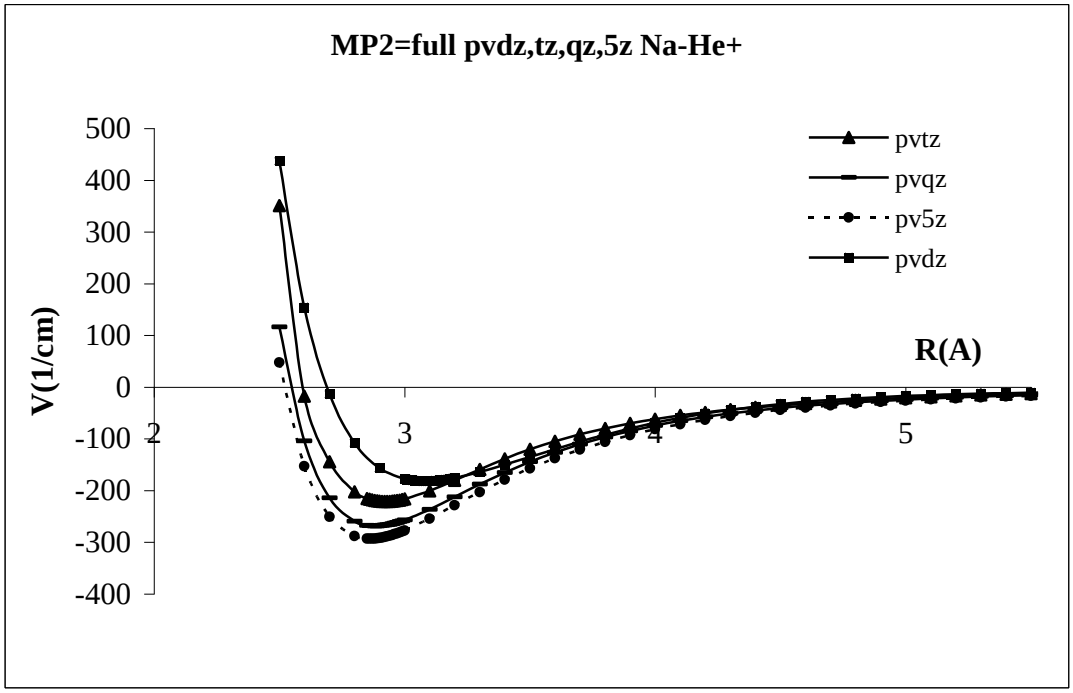

Figure 4.5: PEC of $NaHe^{+}$ obtained from MP2 (full) method with cc-pvdz, pvtz, pvqz, pv5z basis sets.

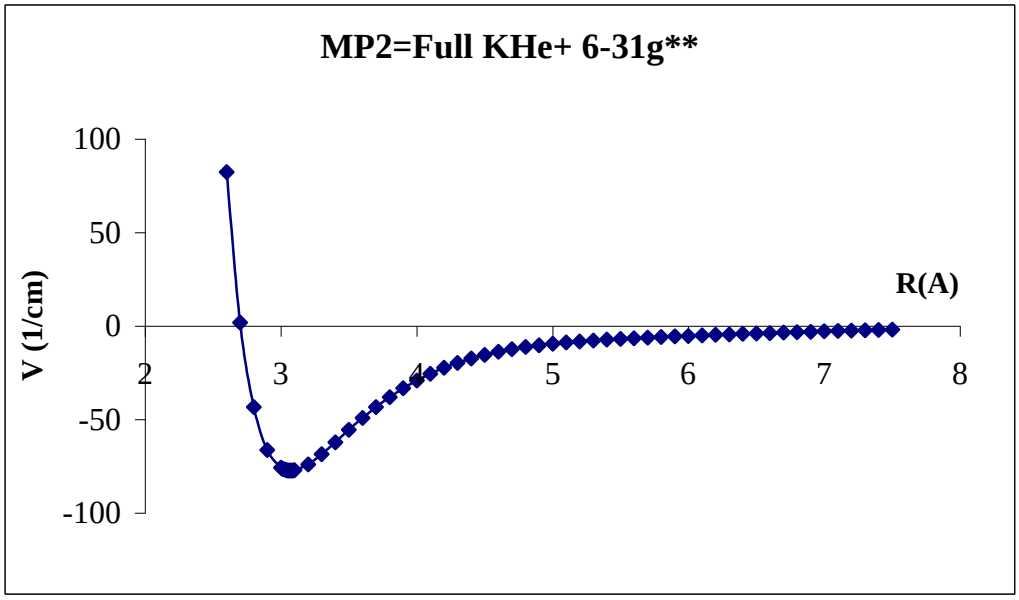

Figure 4.6: PEC of KHe^{+} obtained from MP2 method with 6-31g** basis

Table 4.2: Dissociation energies and bond lengths for $LiHe^+$, $NaHe^+$ and KHe^+ . MP2 (full) results with different basis sets.

MP2=Full		**D_e in (1/cm)**	**R_e(in Å)**
LiHe+	pvdz	348,185	2,13
	Pvtz	539,828	1,93
	pvQz	615,775	1,91
	pv5z	630,080	1,90
	6-311+(3df,3pd)	618.26	1.91
NaHe+	Pvdz	181,934	2,58
	Pvtz	221,172	2,42
	pvQz	268,556	2,38
	pv5z	293,057	2,36
	6-311+(3df,3pd)	381.24	2.342
KHe+	6-31g**	77,282	3,06

In Table 4.2, dissociation energies and bond lengths for $LiHe^+$, $NaHe^+$ and KHe^+ obtained from the MP2 (full) calculations with different basis sets are presented. We see that MP2 (full) method is slightly better than the MP2 method we decided to proceed with MP4 (full) method to increase the quality of the PEC's curves obtained so far. The results are given in Figure 4.7, 4.8, 4.9 for $LiHe^+$, $NaHe^+$ and KHe^+, respectively. The convergence of the R_e and D_e values given in Table 4.3 are much better than the previous results.

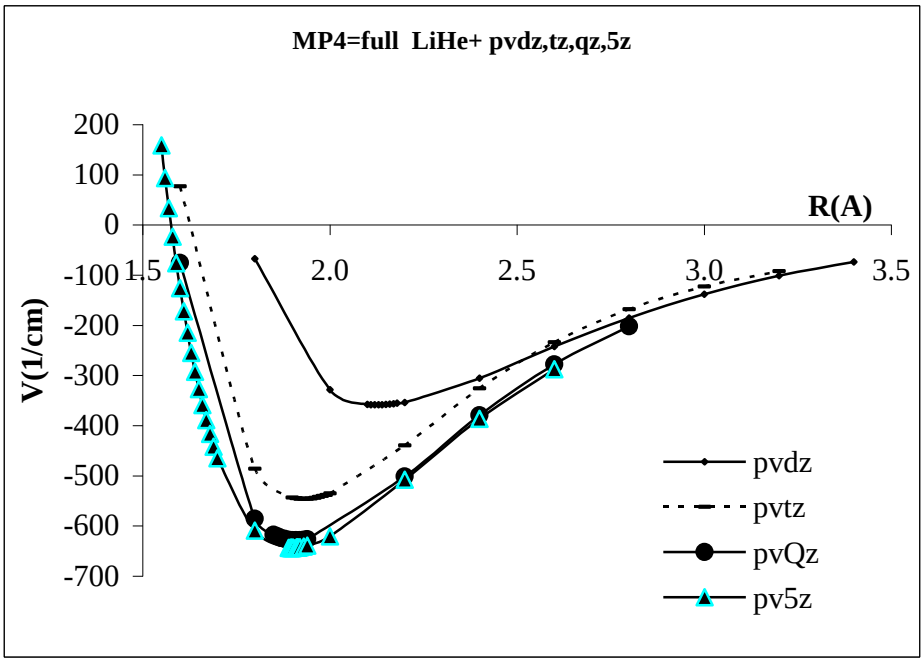

Figure 4.7: PEC of $LiHe^{+}$ obtained from MP4 (full) method with cc-pvdz, pvtz, pvqz, pv5z basis sets.

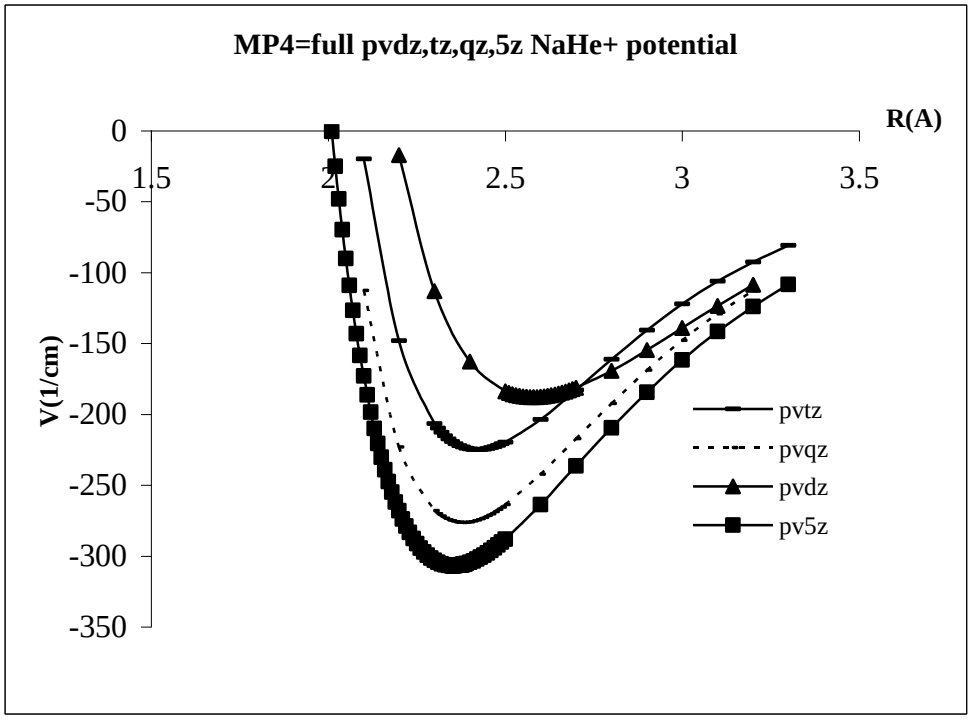

Figure 4.8: PEC of $NaHe^{+}$ obtained from MP4 (full) method with cc-pvdz, pvtz, pvqz, pv5z basis sets.

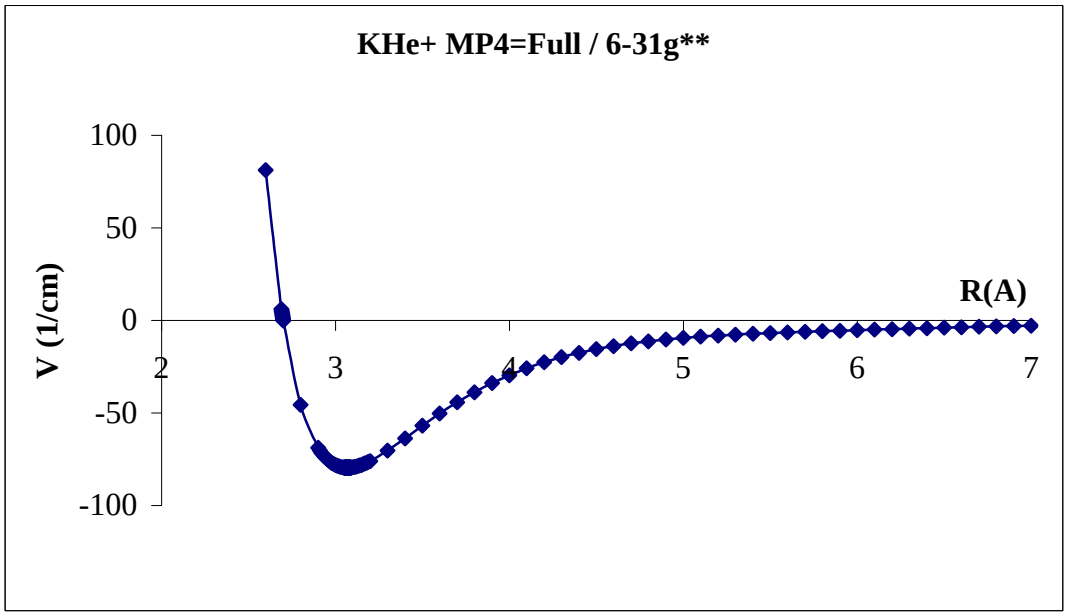

Figure 4.9: PEC of KHe^{+} obtained from MP4 (full) method with cc-pvdz, pvtz, pvqz, pv5z basis sets.

Table 4.3: Dissociation energies and bond lengths for $LiHe^+$,$NaHe^+$ and KHe^+. MP4 (full) results with different basis sets.

MP4=Full		De in 1/cm	Re in Å
LiHe+	pvdz	358,693	2,12
	pvtz	546,3	1,93
	pvQz	628,823	1,91
	pv5z	643,904	1,899
NaHe+	Pvdz	187,923	2,58
	Pvtz	224,926	2,42
	pvQz	276,352	2,38
	pv5z	306,820	2,353
KHe+	6-31g**	79,621	3,068

In MP4 calculations, potential energy is computed at 50 raw points for pvdz, pvtz, pvqz basis functions and at 130 raw points for pv5z basis functions. The reason that we scanned more points for pv5z basis is that this basis provides beter description of PEC in each method. Because of that, the vibrational levels are calculated only for the curves obtained with cc-pv5z basis. Although the potential energy is calculated until the asymptote goes to zero, only the minimum region is shown in the plots to make the differences between the curves more visible.

4.2. CCSD (T) and QCISD (T) calculations

CCSD(T) and QCISD(T) methods are very well known for being very accurate methods for the small systems. we also used these methods to compare to both our MP4 (full) results and the similar results in the literature. The cc-pv5z basis is used for for $LiHe^+$,

$NaHe^+$ and 6-31g** is used for KHe^+ QCISD(T) and 6-311+g(3df, 3pd) is used for KHe^+ CCSD(T). In the Figure 4.10, the PEC's obtained from QCISD(T) calculations and in the Figure 4.11, the PEC's from CCSD(T) calculations are shown. Although all the basis sets are not the same, the reflections of the size effect on the R_e and D_e values given in Table 4.4. can be seen. When compared to MP4(full) method, all three PEC's are simililar in locating the radial minima and in describing the long distance behaviour.

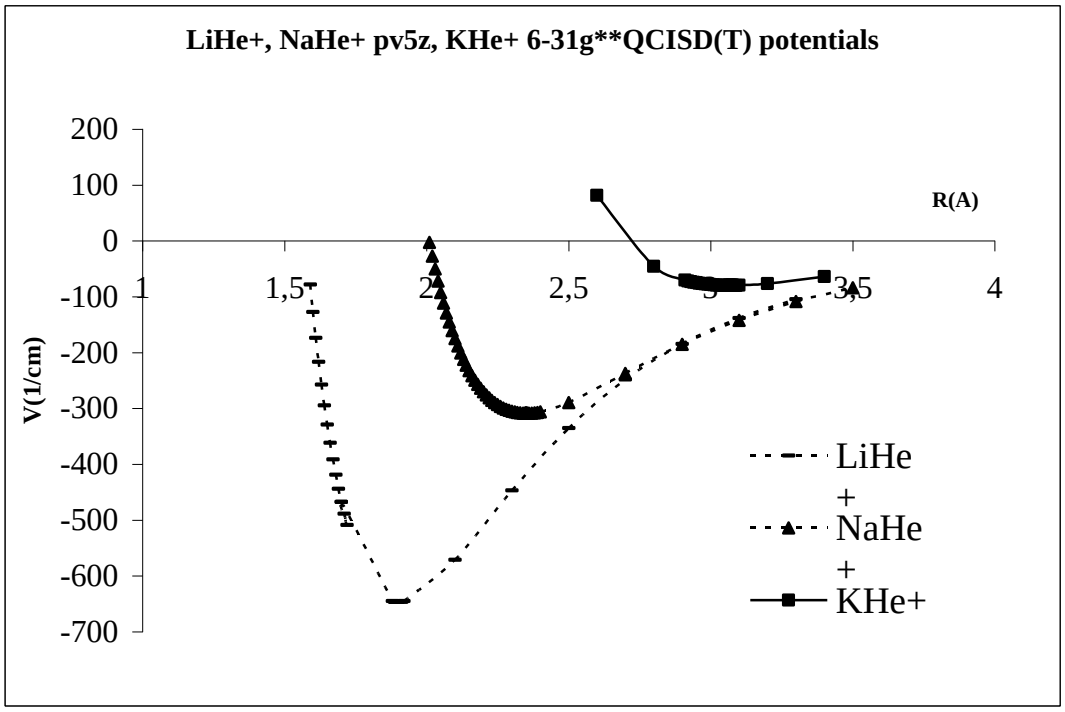

Figure 4.10: PEC 's obtained from QCISD(T) calculations with cc-pv5z basis sets for , $LiHe^+$, $NaHe^+$ and 6-31g** for KHe^+

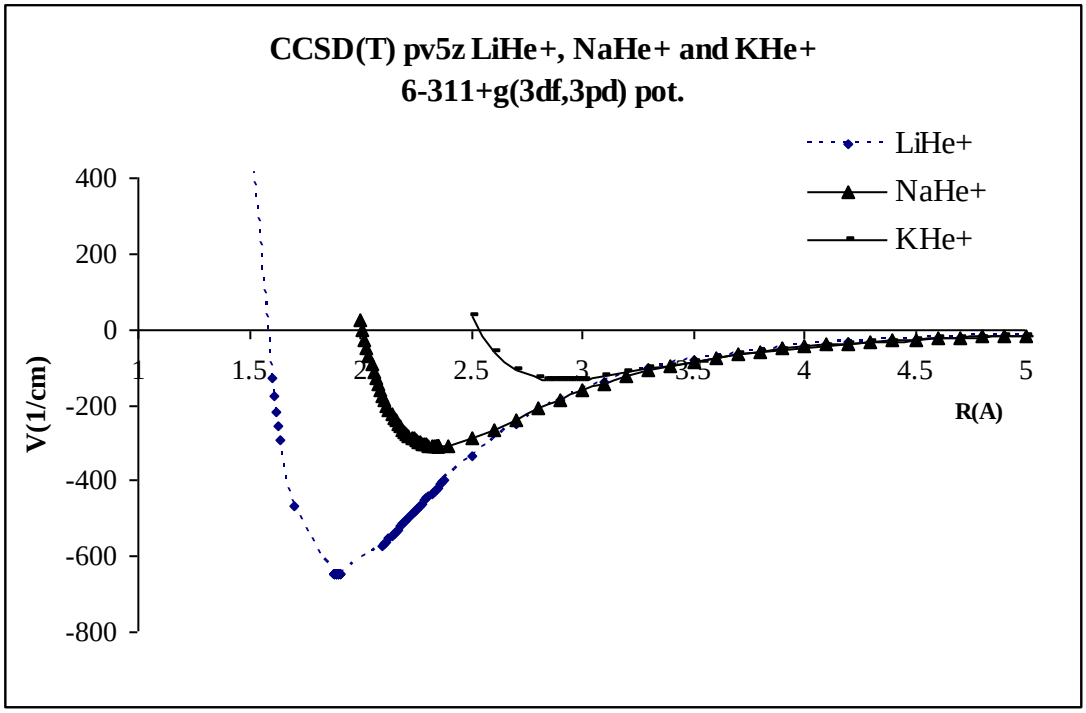

Figure 4.11: PEC 's obtained from CCSD(T) calculations with cc-pv5z basis sets for , $LiHe^+$, $NaHe^+$ and 6-31g** for KHe^+

Table 4.4: Dissociation energies and bond lengths for $LiHe^+$,$NaHe^+$ and KHe^+. QCISD(T) and CCSD(T) results with cc-pv5z basis set.

	Basis Set	QCISD(T)		CCSD(T)	
		De (1/cm)	Re (A^0)	De (1/cm)	Re (A^0)
$LiHe^+$	Pv5z	646,165	1,898	646,168	1,898
$NaHe^+$	Pv5z	308,58	2,352	308,398	2,352
KHe^+	6-31** for QCI 6-311+g for CC	79,844	3,069	136,139	2,90

4.3. DFT/ B3LYP Calculations

The last method we tested is the DFT method. The PEC'S obtained from B3LYP calculations using 6-31g** basis set for all three complexes $LiHe^+$, $NaHe^+$ and KHe^+ are shown in Figure 4.12. The R_e and D_e values are given in Table 4.5. The DFT results are not comparable to the previous results and they give poorer description of such small size systems. The method is good for the larger systems where electron correlations always create a problem. In literature, DFT results are not available.

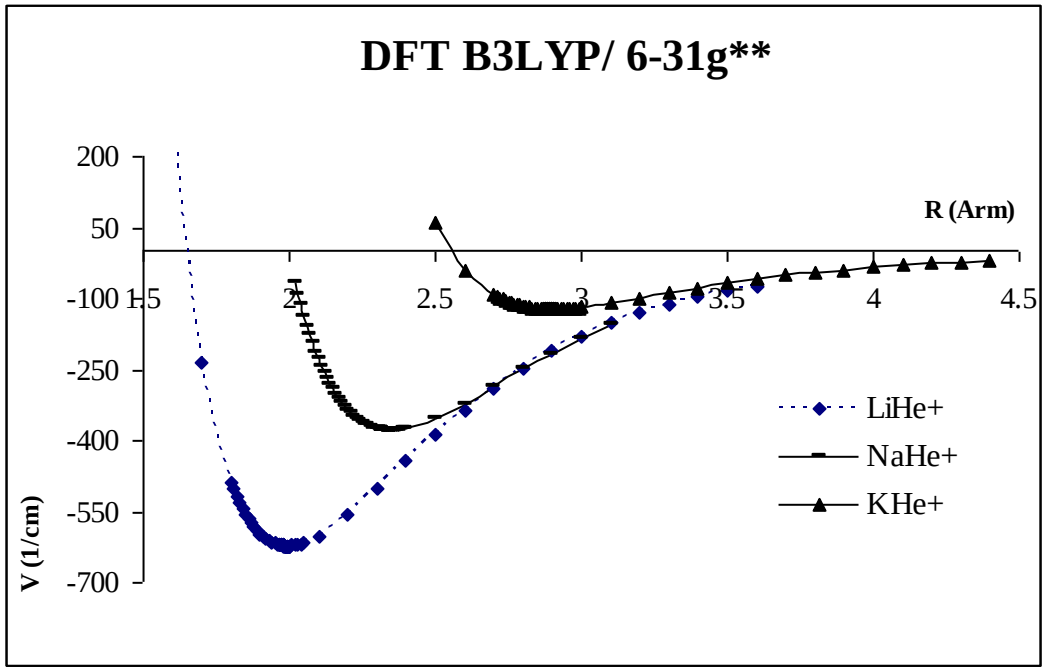

Figure 4.12: PEC 's obtained from B3LYP/6-31g** calculations for $LiHe^+$, $NaHe^+$, KHe^+

Table 4.5: Dissociation energies and bond lengths for $LiHe^+$,$NaHe^+$ and KHe^+. B3LYP/6-31g** results

B3LYP	De (1/cm)	Rm (Arm)
$LiHe^+$	622,264	1,995
$NaHe^+$	378,579	2,349
KHe^+	122,05	2,902

4.4. Comparison of Results

Comparison of our results is given in the Table 4.6 and 4.7. The literature results are given in Table 4.8, Table 4.9, Table 4.10.

Table 4.6: Comparison of the dissociation energies for $LiHe^+$,$NaHe^+$ and KHe^+ with various methods and basis sets

De (in 1/cm)		**Mp2**	**Mp2=full**	**Mp4=full**	**QCISD(T) =full**	**CCSD(T) =full**	**B3LYP 6-31g****
$LiHe^+$	pvdz	345,932	348,185	358,693			622,264
	pvtz	523,713	539,828	546,3			
	pvQz	581,467	615,775	628,823			
	pv5z	584,662	630,080	643,904	646,165	646,168	
$NaHe^+$	pvdz	180,092	181,934	187,923			378,579
	pvtz	209,880	221,172	224,926			
	pvQz	248,814	268,556	276,352			
	pv5z	254,828	293,057	306,820	308,58	308,398	
KHe^+	6-31g	77,29	77,282	79,599	79,844	136,139	122,05

Table 4.7: Comparison of the bond lengths for $LiHe^+$,$NaHe^+$ and KHe^+ with various methods and basis sets

Re (in Å)		**Mp2**	**Mp2= Full**	**Mp4= =full**	**QCISD(T) =full**	**CCSD(T) =full**	**B3LYP 6-31g****
$LiHe^+$	Pvdz	2,14	2,13	2,12			1,995
	Pvtz	1,94	1,93	1,93			
	pvQz	1,93	1,91	1,91			
	Pv5z	1,93	1,90	1,899	1,898	1,898	
$NaHe^+$	Pvdz	2,59	2,58	2,58			2,349
	Pvtz	2,43	2,42	2,42			
	pvQz	2,40	2,38	2,38			
	pv5z	2,41	2,36	2,353	2,352	2,352	
KHe^+	6-31g	3,07	3,06	3,068	3,069	2,90	2,902

For $LiHe^+$, R_e was calculated to be 1.898 Å using the CCSD(T) and QCISD(T) with cc-pV5Z basis sets. R_e was calculated to be 1.904 Å and 1.897 Å using the aug-cc-pVQZ and aug-cc-pV5Z basis sets determined by Soldan [109]. These values compare favorably with the most accurate of previous calculations (a summary of values available up until 1994 has been given by Bililign [51]. We note especially the more recent values of 1.95 Å obtained at the QCISD(T) level [51] using a 6-311G* basis set augmented with three *p* and three *d* functions on He and Li, respectively, and the very recent calculation of 1.894 Å obtained using the extended group function model [52] this is probably the most accurate calculation up to date. It is clear that an extended basis set is required to obtain an accurate bond length in this species. Prior to these studies, the most reliable potentials were the CEPA and CEPA2 potentials of Hariharan and Staemmler [53], and Senff and Burton [54] who obtained R_e values of 1.892 and 1.894 Å, respectively. Our results, together with those of the best of the previous calculations, establish. Re=1.898±0.001

The calculated dissociation energies for $LiHe^+$, D_e for from the present work are 646.165 and 646.168 cm^{-1} using the QCISD(T) and CCSD(T) with cc-pV5Z basis sets, respectively. CCSD (T) calculations of Soldan gives D_e, 637.6 and 649.2 cm^{-1} using the aug-cc-pVQZ and aug-cc-pV5Z basis sets, respectively. These values compare to previous values of 546 cm^{-1} [51], 653 cm^{-1} [52], 649 cm^{-1} [53] and 653 cm^{-1} [54]. Our values, together with the best previous ones establish $D_e(Li^+ \cdot He)$ =645±5 cm^{-1}.

For $NaHe^+$, experimental results calculated by Mason and Viehland [49, 99] seem to be in a good agreement with the our results. R_e was calculated to be 2.353 Å, 2.352 Å, 2.352 Å using the MP4, CCSD (T) and QCISD(T) respectively with cc-pV5Z basis sets. R_e was calculated to be 2.352 Å, 2.303 Å using the aug-cc-pVQZ and U-huz5 (Huzinaga basis set) basis sets determined by Soldan [109]. D_e values also have wide range of results, in comparison to the advanced methods used. This is attributed to the insufficient basis by Ahmadi [142].

After this result we can say that, 6-31g** basis set is too small for KHe^+, 6-311+g(3df, 3pd) gave better results, but as can be seen from Table 4.10, it is still not enough to use for KHe^+_n. Although there has been some earlier theoretical work, we concentrate here on the most recent studies. The first curves we consider are those of Mason, who derived the curve from a ‘‘universal scaling’’ and fitting to available ion mobility data; they obtained *De*= 164 cm^{-1}, and *Re*= 2.91 Å. Moszynski [106] calculated the whole potential using symmetry-adapted perturbation theory (SAPT), and they used the potential to calculate both rovibrational energy levels and transport coefficients. They obtained *De*= 171 cm^{-1}at *Re*=2.87 Å, with the potential being found to support 36 bound rovibrational energy levels. Skullerud and Elford [50,52] used an extended group function (EGF) approach to generate a potential energy curve, obtaining *De*=177.4 cm^{-1} and *Re*=2.85 Å. Best values determined by Soldan for *De* and *Re* are 185.4 cm^{-1} and 2.825 Å.

Table 4.8: Previous studies for dissociation energies and bond lengths of $LiHe^+$

LiHe+	Present Result CCSD(T)	QCISD(T) 6-311+g** [69]	CCSD(T) Aug-Pv5z [109]	CEPA [54]	EGF [52]	MP2=full 6311+g** [69]	Exp [58]
$Re(A^0)$	1,898	1,910	1,897	1,894	1,894	1,910	1,93
$D_e(cm^{-1})$	646,168	630,11	649,155	653	653	618,46	593

Table 4.9: Previous studies for dissociation energies and bond lengths of $NaHe^+$

NaHe+	Present Results CCSD(T)	Exp. [49,58]	QCISD(T) 6-311+g [69]	CCSD(T) Aug-pvQz [68]	CCSD(T) U-huz5 [68]	MP2 6311+g [69]	EGF [67]
$Re(A^0)$	2,352	2,35 2,44	2,334	2,325	2,303	2,342	2,328
$De(cm^{-1})$	308,398	325 276	395,05	329,1	330,7	381,24	326,6

Table 4.10: Previous studies for dissociation energies and bond lengths of KHe^+

KHe+	Present work. CCSD(T)	Exp. [49]	SAPT [106]	CCSD(T) dAug-pv5z [110]	EGF [50]	EGF [108]
$Re(A^0)$	2,90	2.91	2,87	2,825	2,83	2,85
$De(cm^{-1})$	139,198	164	171	185,4	185,5	177,4

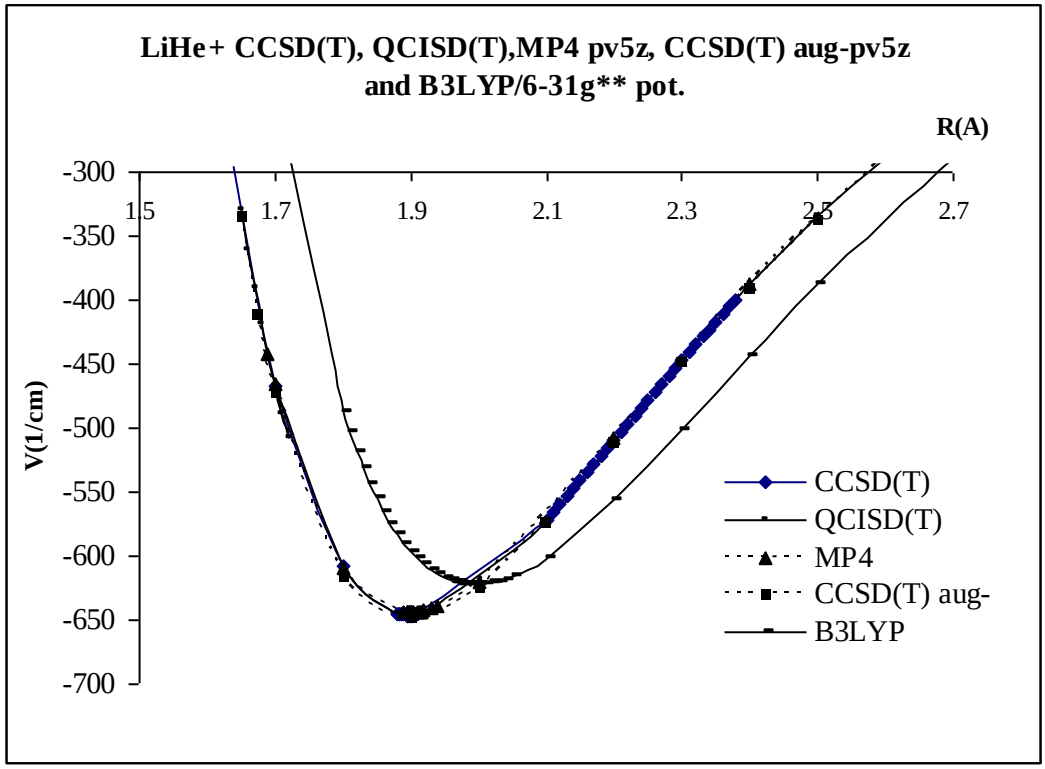

Figure 4.13: $LiHe^+$ potentials as a function of R by using various methods and basis sets

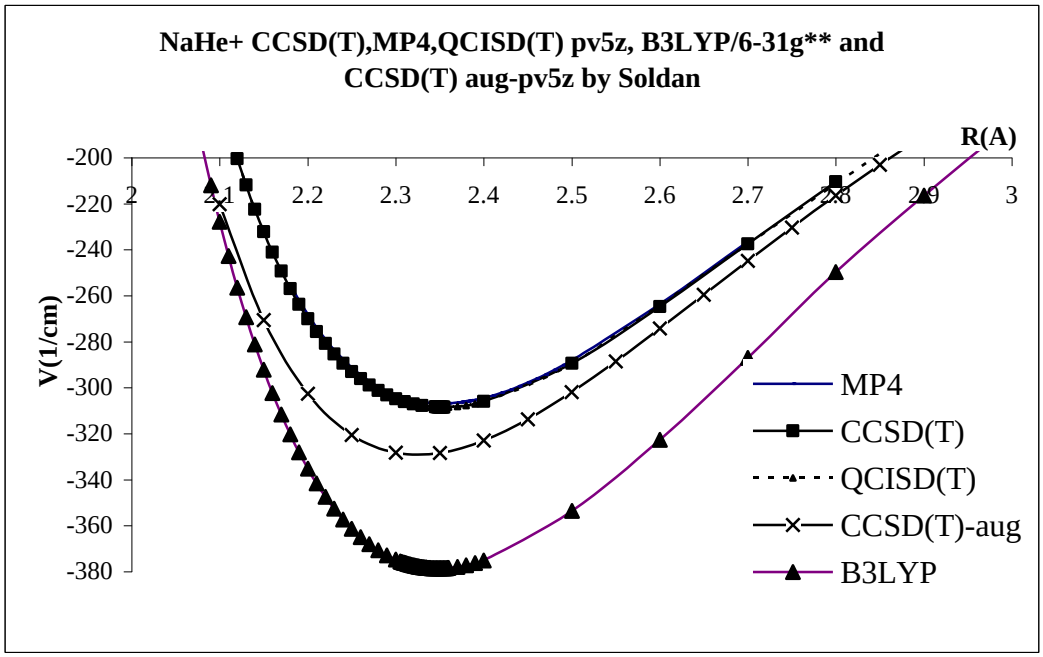

Figure 4.14: $NaHe^+$ potentials as a function of R by using various methods and basis sets

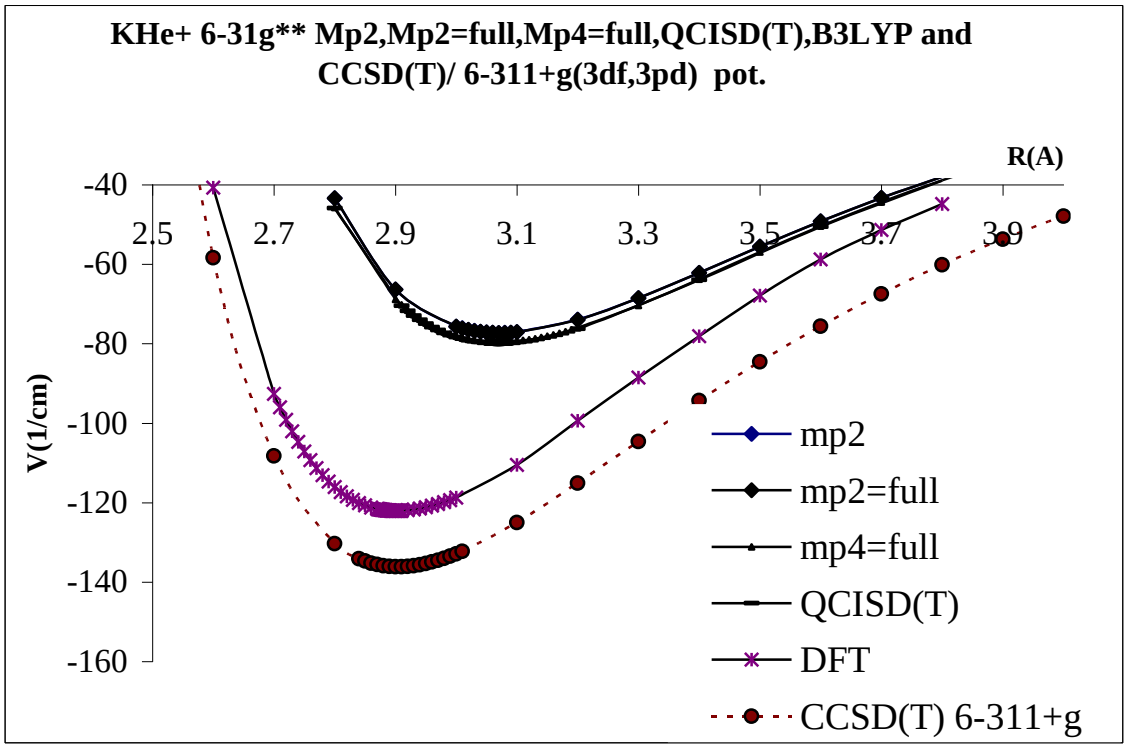

Figure 4.15: KHe^{+} potentials as a function of R by using various methods and basis sets

Comparing the methods in CPU time; MP4, QCISD(T), CCSD(T) methods that we determine as consistent methods for our systems, are very expensive in time. As we expect DFT is much more cheaper. In addition to that we have to calculate potentials for over hundred points to determine bound vibrational and rovibrational states exactly. It is known that QCISD methods are slightly cheaper than CCSD(T). Although we found same results for monocations, we know that CCSD(T) would give better results for these kind of systems. Next, its computational effort is much better.

For basis set comparison, 6-31g** and 6-311+g(3df,3pd) basis set which is not give suitable results are cheaper ones. Dunnings consistent correlated basis sets seems to increase in CPU time with pvdz<pvtz<pvqz<pv5z which is the respectively give the complexness of basis sets, as expected. Augmented basis sets which prefixed by aug- used before these systems, is the most expensive one and it will be hard to perform this basis set to He complexed with more than one

Table 4-11: Comparison of Methods and Basis sets in CPU times

Molecule	Method	Basis Set	Number of points	CPU Time Day-Hour-Min.
$LiHe^+$	MP2	pvQz	31	00-04-33
	MP2	pv5z	31	00-18-33
	MP2=full	pvQz	31	00-03-57
	MP2=full	pv5z	31	00-21-02
	MP4=full	Pvdz	31	00-00-25
	MP4=full	pvtz	31	00-00-48
	MP4=full	pvQz	31	00-10-28
	MP4=full	pv5z	31	01-14-19
	QCISD(T)	pv5z	31	05-06-39
	CCSD(T)	pv5z	21	02-03-14
	CCSD(T)	aug-pv5z	21	11-02-10
	B3LYP	6-31g**	21	00-01-40
$NaHe^+$	MP2	pvQz	36	00-13-50
	MP2	pv5z	36	01-11-37
	MP2=full	pvQz	36	00-23-20
	MP2=full	pv5z	36	01-14-19
	MP4=full	pvQz	36	00-20-49
	MP4=full	pv5z	41	09-05-01
	QCISD(T)	pv5z	36	04-17-16
	CCSD(T)	pv5z	40	06-12-59
	B3LYP	6-31g**	36	00-03-04
KHe^+	MP2	6-31g**	41	00-05-00
	MP2=full	6-31g**	41	00-05-16
	MP4=full	6-31g**	41	00-05-54
	QCISD(T)	6-31g**	26	00-03-54
	CCSD(T)	6-311+g	30	01-09-51
	B3LYP	6-31g**	41	00-03-50

4.5. Bound Vibrational Levels and Charges

Le Roy's LEVEL program[112] was used to calculate vibrational energy levels for J=0 for CCSD(T), QCISD(T) and MP4 calculations with cc-pc5z basis set.

The results for are given in the Table 4.11 and Table 4.12. The last columns are the reference values from Soldan. [2,3]

The results especially one of the first vibrational bound states are very close to the reference. But still we could not determine the 8.th vibrational state for $LiHe^+$ and 7.th one for $NaHe^+$ that the basis set difference causes them to be very close to the zero, so we could not determine it with our significant figures.

Table 4.12: Bound vibrational energy levels for the $LiHe^+$ complexes.

$LiHe^+$ v	CCSD(T) cc-pv5z	MP4=full cc-pv5z	QCISD(T) cc-pv5z	CCSD(T)[109] Aug-pv5z
0	-517.445	-515.258	-517.371	-519,925
1	-308,892	-307.23	-308.848	-311,396
2	-162,666	-161.554	-162.638	-165,739
3	-71.154	-70.498	-71.142	-75,323
4	-23,454	-23.146	-23.45	-27,55
5	-4,734	-4,637	-4.733	-7,191
6	-0,328	-0.315	-0.328	-0,925
7				-0,007

Table 4.13: Bound vibrational energy levels for the $NaHe^+$ complexes.

$NaHe^+$ v	CCSD(T) cc-pv5z	MP4=full cc-pv5z	QCISD(T) cc-pv5z	CCSD(T) [68] Aug-pv5z
0	-237,891	-236.125	-237.679	-255,18
1	-129,136	-127.794	-128.865	-141,47
2	-59,521	-58.554	-59.209	-68,75
3	-21,652	-20.977	-21.296	-28,3
4	-5,782	-5.284	-5.4	-9,05
5	-1,053	-0.635	-0.659	-1,85
6	-0,31			-0,13

Because in comparison with pv5z basis set, the basis set 6-311+g (3df, 3pd) does not correctly define KHe^+ system which includes higher number of electrons, the vibrational bound levels are not be found near to the ones in the literature as can be seen in the Table 4.14.

Table 4.14: Bound vibrational energy levels for the KHe^+ complexes.

$NaHe^+$ v	CCSD(T) cc-pv5z [110]	CCSD(T) 6-311+g (3df,3pd)
0	-136,930	-96,097
1	-66,873	-41,519
2	-27,203	-13,455
3	-8,630	-2,156
4	-1,781	-0,238
5	-0,136	

Mulliken charges on the atoms are given in Table 4.14 for CCSD(T) method, Results are very similar for other methods. Because of the atomic sizes, as the charge on the He complexed with the Li^+ is highest, as we expect.

Table 4.15: Calculated Mulliken charges on the atoms for CCSD(T) method

Mulliken Atomic charges(a.u)	$LiHe^+$	$NaHe^+$	KHe^+
Metal	0.938776	0.965830	0.987488
He	0.061224	0.034170	0.012512

5. CONCLUSION

This work was motivated by experimentalists who needed new theoretical studies that will help in the interpretation of the wealth of information contained in spectroscopic parameters in terms of microscopic interactions of the impurities embedded in helium clusters. The first step in cluster studies is to understand the diatomic interactions between the He atom and the impurity, which is, in our study, a positively charged metal of group 1. The theoretical calculations using advanced post-HF methods and reasonably large basis sets such as cc-pv5z have been carried out to calculate the spectroscopic constants for the ground electronic state of the $LiHe^+$, $NaHe^+$, and KHe^+ diatomic complexes. It has been found that the complexes are still stable after including zero-point-energy corrections. Strong correlation between the binding energy and bond length was observed since the bonding is predominantly electrostatic due to the charge-induced dipole of the cation. Calculated dissociation energies and bond lengths were observed to be in a very good agreement with the experimental values for $LiHe^+$, in a good agreement for $NaHe^+$. %15 error in dissociation energy and less than % 0.4 in bond length was obtained for KHe^+. This error was attributed to the insufficient basis set or lack of diffusion functions used for KHe^+. Vibrational energy levels have been seen to be more sensitive to the accuracy of the PEC and low lying states can be calculated more accurately than the higher vibrational levels since they are noticably dependent on the long range interaction of the adducts. The increase in the bond lengths and the dramatical decrease in dissociation energies was obtained as the size of the metal increases. The polarization effects of the larger cations became weaker and that was reflected on the charge densities. For $NaHe^+$ and KHe^+ cases , the positive charge of the complexes localized on the metal.

Several methods have been employed to see the differences in the PECs of the molecules under consideration. DFT methods turned out to be inadequate in describing the interactions. MP4 (full), QCISD(T) and CCSD(T) methods with cc-pv5z basis are

similar in quantitative description of these diatomic systems. Although the aug-cc-pv5z basis is much better, the computation time can not be affordable for studying the larger clusters. Coupled Cluster method with pv5z basis are the most suitable method when considered on a quality versus computation time basis. For a better description of PEC of KHe^+, the augmented cc-pv5z basis must be used. With the informations extracted from this study, the stability, the shape and the solvation shell of larger $LiHe_n^+$, $NaHe_n^+$, and KHe_n^+ clusters with n=2, 3… will be carried out.

As the size of the metal increases, Re increases, number of bound vibrational levels decreases, the charge localization on the metal ion decreases, the potential energy curve becomes more shallow and the bond dissociation energy decreases drastically, the interaction between M+ and He weakens, M+ and He interaction resembles to He – He interaction and the quantum effects become more appreciable.

REFERENCES

[1] **Whittle, E., Dows, D.E. and Pimentel G.C.**, 1954. Matrix isolation method for the experimental study of unstable species, *J. Chem. Phys.*, **22**,1943-1949.

[2] **Andrews, L., Moskovits**, M., 1989. Chemistry and Physics of Matrix isolated Species, North Holland, Amsterdam.

[3] **Jacox, M.E.**, 1984. Ground-State Vibrational Energy Levels of Polyatomic Transient Molecules, *J. Phys. Chem. Ref. Data*, **13**, 945-958.

[4] **Jacox, M.E.,** 1988. Electronic Energy Levels of Small Polyatomic Transient Molecules, *J. Phys. Chem. Ref. Data*, **17**, 269-279.

[5] **Toennies, J.P., Vilesov, A.F**., 1998. Spectroscopy of atoms and molecules in liquid Helium, *Annu. Rev. Phys. Chem*., **49**, 1-41.

[6] **Toennies, J.P., Vilesov, A.F., Whaley, K.B**., 2001. Superfluid Helium Droplets: An Ultracold Nanolaboratory, *Phys. Today*, **2**, 31-38.

[7] **Northby, J.A.,** 2001. Experimental studies of helium droplets, *J. Chem. Phys.*, **115**, 10065-72.

[8] **Callegari, K., Lehmann, K.K., Schmied, R., Scoles, G.,** 2001. Helium nanodroplet isolation rovibrational spectroscopy: Methods and recent results, J. Chem. Phys., **115**, 10090-98.

[9] **Stienkemeier, F., Vilesov, A.F.,** 2001. Electronic spectroscopy in He droplets, *J. Chem. Phys*., **115**, 10119.

[10] **Toennies, J.P., Vilesov, A.F.,** 2004. Superfluid Helium Droplets: A Uniquely Cold Nanomatrix for Molecules and Molecular Complexes, *Angewandte Chemie*., **43**, 2622-2649.

[11] **Kiryukhin, V., Keimer, B., Boltnev, R.E., Khmelenko, V.V., Gordon, E.B.,** 1997. Inert-Gas Solids with Nanoscale Porosity, *Phys. Rev. Lett.*, **79**, 1774-1782.

[12] **Yabuzaki, T., Fujisaki, A., Sano, K., Kinoshita, T., Takahashi**, **Y.,** 1997. Physics of Atoms in Superfluid Helium , *Atomic Physics*, **13**, 337-348.

[13] **Kanorsky, S.I., Weis, A., 1996.** in *Quantum Optics of Confined Systems*, Eds.: M. Ducloy, D. Bloch, Kluwer, Dordrecht.

[14] **Tabbert, B., Gunther, H., zu Putlitz, G.,** 1997. Lifetimes of metastable magnesium atoms in He, *J. LowTemp. Phys.*, **109**, 653-664.

[15] **Ghazarian, V., Eloranta, J., Apkarian, A.,** 2002. Universal molecule injector in liquid helium: Pulsed cryogenic doped helium droplet source, *Rev. Sci. Instrum*., **73**, 3606-3612.

[16] **Foerste, M., Gunther, H., Riediger, O., Wiebe, J., zu Putlitz, G.,** 1997. Optical and mobility measurements of alkali earth atoms and ions in superuid helium, *Z. Phys. B.* **104**, 317–322

[17] **Glaberson, W.I. , Johnson, W.W**., 1997, Equilibrium vortex density in a rotating two dimentional superfluid, *J. Low Temp. Phys.*, **20**, 313–338

[18] **Claas, P., Mende, S.O., Stienkemeier, F.,** 2003. Characterization of laser ablation as a means for doping helium nanodroplets**,** *Rev. Sci. Instrum.* **, 74,** 4071.

[19] **Atkins, K.P.,** 1959. Ions in Liquid Helium, *Phys. Rev*., **116**, 1339

[20] **Jortner, J., Kestner, N.R., Rice, S.A., Cohen, M.H.,** 1965. Study of the Properties of an Excess Electron in Liquid Helium. I. The Nature of the Electron—Helium Interactions *J. Chem. Phys.* **43,** 2614–2625.

[21] **Fowler, W.B., Dexter, D.L**., 1968. Electronic Bubble States in Liquid Helium, *Phys. Rev.*,**176**, 337–343

[22] **Rosenblit, M., Jortner, J**., 1997. Dynamics of Excess Electron Localization in Liquid Helium and Neon, *J. Phys.Chem. A,* **101**, 751– 757

[23] **Padmore, T.C., Cole, M.W.,** 1974. Free surface of He II and the electron bubble, *Phys. Rev. A,* **9**, 802–807.

[24] **Cole MW, Bachman RA**., 1977. Structure of positive impurity ions in liquid helium, *Phys. Rev. B,* **15**, 1388–1394.

[25] **Cole, M.W., Toigo, F**., 1978. Structural transition for positive impurity ions in fluids, *Phys. Rev. B,* **17**, 2054–2056

[26] **Ott-Rowland ML, Kotsubo V, Theobald J, Williams GA.** 1982. Two-Dimensional Plasma Resonances in Positive Ions under the Surface of Liquid Helium, *Phys. Rev. Lett.***49**:1708–12

[27] **Steets, W., Hickman, A.P., Lane, N.F**., 1974. Theoretical description of pressure shifts and quenching of excited atomic states in liquid helium, *Chem. Phys. Lett.*, **28**, 31–34.

[28] **Hickman, A.P., Steets, W., Lane, N.F.,** 1975. Nature of excited helium atoms in liquid helium: A theoretical model, *Phys. Rev. B* **12**, 3705–3717

[29] **Wisdom J, Hartquist TW, Lane NF**. 1976. He(2^3S) bubble in liquid helium, *Phys. Rev. B*, **14**, 4205–4208

[30] **Kanorsky, S.I., Arndt, M., Dziewior, R., Weis, A., Hansch, T.W.,** 1994. Pressure shift and broadening of the resonance line of barium atoms in liquid helium, *Phys. Rev. B,* **50**, 6296–6302

[31] **Kinoshita, T., Fukuda, K., Takahashi, Y., Yabuzaki, T.,** 1995. Optical properties of alkali-metal atoms in pressurized liquid helium, *Phys. Rev.A,* **52**, 2707– 2716

[32] **Kinoshita, T., Fukuda, K., Yabuzaki, T**., 1996. Doubly shaped D_2 excitation spectra of Cs and Rb atoms in superfluid helium due to a quadrupole bubble surface oscillation, *Phys. Rev. B,* **54**, 6600–6607

[33] **Bauer, H., Beau, M., Friedl, B., Marchand, C., Miltner, K., Reyher, H.J**., 1990. Laser spectroscopy of Alkaline Earth ions in HeII, *Phys. Lett.*, **146**, 134–140

[34] **Zu Putlitz, G., Beau, M**., 1992. In *Topics in Applied Physics*, ed. M Stuke, **70**, 237– 247., Springer-Verlag, Berlin, Heidelberg

[35] **Beau, M., Gunther, H., zu Putlitz, G., Tabbert, B.,**1996. *Z. Phys. B,* **101**, 253–262.

[36] **Tang, J.Z., Kimura, M., Shimamura, I**., 1996. Absorption and emission spectra of alkaline-earth atoms in liquid helium: a theoretical study**,** *Chem. Phys. Lett.* **256**, 327–333.

[37] **Whaley, K.B.,** 1997. In *Advances in Molecular Vibrations and Collision Dynamics*, ed. by J Bowman, Vol. **3**: *Molecular Clusters*, Greenwich.

[38] **Whaley, K.B.,** 1994. Structure and dynamics of quantum clusters**,** *Int. Rev. Phys. Chem.,* **13**, 41–84.

[39] **McMahon, M.A., Whaley, K.B.**, 1995. Quantum Monte Carlo studies of anisotropy and rotational states in He_NCl_2, *J. Chem. Phys.,* **103**, 2561–2571.

[40] **Galli, D.E., Buzzacchi, M., and Reatto, L., 2001.** Pure and alkali–ion-doped droplets of ^{4}He, *J. Chem. Phys.,* **115**, 10239.

[41] **Ishikawa, K., Hatakeyama, A., Gosyonoo, K., Wada, S., Takahashi, Y., Yabuzaki, T.,** 1997. Laser spectroscopy of thulium atoms implanted in liquid and solid ^{4}He, *Phys. Rev. B,* **56**, 780–787.

[42] **Arndt, M., Dziewior, R., Kanorsky, S., Weis, A., Hansch, T.W**., 1995. Implantation and Spectroscopy of Metal Atoms in Solid Helium, *Z. Phys. B,* **98**, 377– 381.

[43] **Beau, M., Fischer, J., zu Putlitz, G., Reyher, H.J., Schreck, H**., 1991. *Proc. Int. Conf. Coherent Nonlinear Optics ICONO **91***, 14th, St. Petersburg, Russia.

[44] **Takahashi, N., Shimoda, T., Miyatake, H., Mitsuoka, S., Mizoi, Y.**,1996. Radioactive Core Ions of Microclusters, ``Snowballs'' in Superfluid Helium **,** *Hyperfine Interact*., **98**, 469–477.

[45] **Persson, J.L., Hui, Q., Nakamura, M., Takami, M., 1995**. Optical spectra of metal dimers and trimers in superfluid helium, *Phys. Rev. A,* **52**, 2011–2015.

[46] **Gunther, H., Foerste, M., zu Putlitz, G., Schumacher, T**., 1996. **Low temperature physics**, superconductivity, and superfluidity, *Low Temp. Phys.*, **22**, 143–147.

[47] **Maroulis, G. and Thakkar**, **A.J.,** 1989. Hyperpolarizabilities and polarizabilities of neon: Discrepancy between theory and experiment**,** *Chem. Phys. Lett.*, **156**, 87-94.

[48] **Tang, K.T., Norbeck, J.M. and Certain**, J.R., 1976. Upper and lower bounds of two- and three-body dipole, quadrupole, and octupole van der Waals coefficients for hydrogen, noble gas, and alkali atom interactions, *J. Chem. Phys*., **64**, 3063-3074.

[49] **Koutselos, A.D., Mason, E.A.and Viehland, L.A., 1990.** Interaction universality and scaling laws for interaction potentials between closed-shell atoms and ions, *J. Chem. Phys***., 93,** 7125-7134**.**

[50] **Skullerud, H.R., Løvaas, T.H. and Tsurugida, K.,** 1999. Interaction potential and transport coefficients for Na+ ions in helium, *J. Phys. B,* **32**, 4509-4516.

[51] **Bililign, S., Gutowski, M., Simons, J. and Breckenridge, W.H.,** 1992. Potential energy curves of M($np\ ^2P$)·RG($^2\pi$) excited states and M^+ ·RG ground states (M=Li, Na; RG=He, Ne) *J. Chem. Phys.*, **100**, 8212-8225.

[52] **Elford, M.T., Røeggen, I. And Skullerud, H.R., 1999,** Interaction potential and transport coefficients for Li+ ions in helium, *J. Phys. B* ., **32**, 1873-1894.

[53] **Hariharan, P.C. and Staemmler, V., 1999.** Transport coefficients and interaction potentials for Li^+ , *Chem. Phys.*, **15**, 409-419.

[54] **Senff, U.E. and Burton, P.G., 1999.** A cepa2 investigation of He-He and He-Li+ potentials, *Mol. Phys.*, **58**, 637-645.

[55] **Tang, K.T. and Toennies, J.P.,** 1984. An improved simple model for the van der Waals potential based on universal damping functions for the dispersion coefficients *J. Chem. Phys.*, **80,** 3726-3737.

[56] **Tang, K.T. and Toennies, J.P.,** 1986. New combining rules for the well parameters and shapes of the van der waals potential of mixed rare gas systems, *Z. Phys. D*., **1**, 91-98.

[57] **Takebe, M.,** 1983. The generalized mobility curve for alkali ions in rare gases: Clustering reactions and mobility curves, *J. Chem. Phys.*, **78,** 7223-7229.

[58] **Viehland, L. A**., 1984. Interaction potentials for Li+-Rg systems, *Chem. Phys.*, **85,** 291-298.

[59] **Buzzacchi, M., Galli, D.E., Reatto**, L., 2001. Alkali ions in superfluid ^{4}He and structure of the snowball, *Phys. Rev. B.*, **64**, 094512.

[60] **Rossi, M., Verona, M., Galli, D.E., Reatto, L.,** 2004, Alkali and alkali-earth ions in ^{4}He systems, *Phys. Rev. B.***, 69,** 212510

[61] **Partridge, H., Bauschlicher, C.W., Jr. and Langhoff**, S.R., 1992. Theoretical study of metal ions bound to helium, neon, and argon**,** *J. Phys. Chem*., **96**, 5350-5357.

[62] **Koutselos, A.D. and Mason**, **E.A.,** 1986. Correlation and prediction of dispersion coefficients for isoelectronic systems, *J. Chem. Phys*., **85**, 2154-2160.

[63] **Fuentaelba**, 1986. Calculation of alkali-ion-rare-gas potentials: the LiHe+ ion, *J. Phys. B: At. Mol. Phys*., **19**, 235-239.

[64] **Ong, P.P. , Hogan, M.J. , Tan**, **T.L. ,**1992**.** Reexamination of the Li+-He interaction potential, *Physical Review A.*, **9**, 5707-5718.

[65] **Larsen**, 1988, Transport coefficients and interaction potentials for lithium ions in helium and argon, *J. Phys. B*, **21**, 2519-2527.

[66] **Ahlrich, R., Bijhm, H. J., Brode, S., Tang, K. T. and Toennies**, **J. P.,** 1988. Interaction potentials for alkali ion–rare gas and halogen ion–rare gas systems, *J. Chem. Phys*., **88**, 6290-6299.

[67] **Bodo, E., Gianturco, F.A., Sebastianelli, F., Yurtsever, E. and Yurtsever, M.,** 2004. Ab initio quantum dynamics with very weak van der Waals interactions: Li_2 ($1\Sigma g+$)He_2 clusters, *J. Chem. Phys*., **120**, 9160.

[68] **Soldan, P., Lee, E. P. F. and Wright T. J.,** 1999, Interatomic potentials for the Na+-Rg complexes (Rg = He , Ne and Ar), *Mol. Phys.* **97**, 139.

[69] **Sapse, A., Dumitra, A., Jain, D.C**., 2003, A theoretical study of $LiHe_n+$, $NaHe_n+$, and $MgHe_n+$ complexes, with n = 1, 2, 3, 4, *Journal of Cluster Science*, **14**, 1-21.

[70] **Jacox, M. E.,** 1994. The vibrational energy levels of small transient molecules isolated in Neon and Argon matrices**,** *Chem. Phys*., **189**, 149-161.

[71] **Wilks, J., Betts**, **D.S.,** 1987. An Introduction to Liquid Helium, Clarendon Press, Oxford.

[72] **Toennies, J.P., Vilesov, A.F.,**1998. Spectroscopy of atoms and molecules in liquid Helium, *Annu. Rev. Phys. Chem*., **49**, 1-11.

[73] **Silvera, I. F.,** 1988. Ultimate fate of a gas of atomic hydrogen in a liquid-helium chamber: Recombination and burial, *Phys. Rev. B***, 29,** 3899-3906.

[74] **Apkarian, V.A. and Schwentner**, **N.,** 1999. Molecular Photodynamics in Rare Gas Solids, *Chem. Rev*., **99**, 1481-1489.

[75] **Fetter**, **A.L.,** 1976. In The Physics of Liquid and Solid Helium, edited by K. H. Bennemann, J. B. Ketterson, Wiley, New York.

[76] **Takahashi, N.,** 2000, Condensed-matter nuclear physics with radioactive beams snowballs in superfluid helium, *Physica B*., **89**, 284-295.

[77] **H. Kamerlingh Onnes**, 1998. Commun. Phys. Lab. Univ. Leiden, **105**, 744-755.

[78] **Kim, H., Seo, K., Tabbert, B. and Williams**, **G. A.,** 2002. Properties of superfluid fog**,** *Europhys. Lett*., **58**, 395-405.

[79] **Weilert, M.A., Whitaker, D. L., Maris, H.J. and Seidel**, **G. M.,** 1995. Laser levitation of superfluid helium, *J. Low Temp. Phys*., **98**, 17-31.

[80] **Weilert, M. A., Whitaker, D. L., Maris, H. J. and Seidel**, **G.M.,** 1996. Magnetic Levitation and Noncoalescence of Liquid Helium, *Phys. Rev. Lett*., **77**, 4840-4851.

[81] **Tsao, C.C., Lobo, J.D., Okumura, M., Lo, S.Y.**, 1998. Generation of charged droplets by field ionization of liquid helium, *J. Phys. D*, **31**, 2195-2206.

[82] **Becker, E.W., Klingelhöfer, R. And Lohse, P., 1961.** Strahlen aus kondensiertem Wasserstoff, kondensiertem Helium und kondensiertem Stickstoff im Hochvakuum, *Naturforsch. A*, **16**, 1259-1267.

[83] **Buchenau, H., Knuth, E.L., Northby, J., Toennies, J. P. and Winkler, C. 1990.** Mass spectra and time-of-flight distributions of helium cluster beams, *J. Chem. Phys*., **92**, 6875-6882.

[84] **Buchenau, H, Northby, J., Toennies, J. P., 1991,** Excitation and ionization of ^{4}He clusters by electrons, *J. Chem. Phys*., **95**, 8134-8145.

[85] **Harms, J., Toennies, J. P., Dalfovo, F., 1998.** Density of superfluid helium droplets, *Phys. Rev. B*, **58**, 3341-3350.

[86] **Harms, J., Toennies, J. P., 2001.** Experimental and theoretical study of the radial density distributions of large ^{3}He droplets, *Phys. Rev. B*, **63**, 184513.

[87] **Lewerenz, M., Schilling, B., Toennies**, **J.P.,1993.** A new scattering deflection method for determining and selecting the sizes of large liquid clusters of ^{4}He, *Chem. Phys. Lett*., **206**, 381-389.

[88] **Slipchenko, M., Kuma, S., Momose, T., Vilesov, A. F.,** 2002, Intense pulsed helium droplet beams, *Rev. Sci. Instrum*., **73**, 3600-3608.

[89] **Gough, T.E., Mengel, M., Rowntree, P.A., Scoles, G.,** 1985. Infrared spectroscopy at the surface of clusters: SF_6 on Ar, *J. Chem. Phys*., **83**, 4958-4965.

[90] **Gspann**, **J., 1981.** Helium microdroplet transparency in heavy atom collisions, *Physica B+C*, **108**, 1309-1317.

[91] **Scheidemann, A., Toennies**, **J. P., Vilesov, A. F.,** Northby, J. A., 1990. Capture of neon atoms by ^{4}He clusters, *Phys. Rev. Lett*., **64**, 1899-105.

[92] **Lindinger, A. and Toennies**, **J. P.,** 1999. High resolution vibronic spectra of the amino acids tryptophan and tyrosine in 0.38 K cold helium droplets, *J. Chem. Phys*., **110**, 1429-1439.

[93] **Levis**, R.J., 1994. Laser desorption and ejection of biomolecules from the condensed phase into the gas phase, *Annu. Rev. Phys. Chem*., **45**, 483.

[94] **Lewerenz, M., Schilling, B., Toennies**, **J.P.,** 1995**.** Successive capture and coagulation of atoms and molecules to small clusters in large liquid helium clusters, *J. Chem. Phys.*, **102**, 8191-8200.

[95] **Hartmann, M., Miller, R., Toennies**, **J.P., Vilesov, A.F.**, 1996. High-resolution molecular spectroscopy of van der Waals clusters in liquid helium droplets, *Science*, **272**, 1631-1637.

[96] **Gianturco, F.A.,** 1976. Potential energy curves from the electron gas model. II. The ion–rare gas interactions, *J. Chem. Phys*., **64**, 1973-1980.

[97] **Kim, Y.S. and Gordon G.R**., 1972. Unified theory for the intermolecular forces between closed shell atoms and ions, *J. Chem. Phys*., **61**, 1-10.

[98] **Viehland, L.A. and Mason**, **E.A.,** 1975, Gaseous Ion Mobility in Electric Fields of Arbitrary Strength, *Ann. Phys.*, **91**, 499-508.

[99] **Gartland, I.R., Viehland, L.A., Mason**, **E.A., 1977.** Tests of alkali ion-inert gas interaction potentials by gaseous ion mobility experiments, *J. Chem. Phys*., **66**, 537-548.

[100] **F. E. Budenholzer, E. A. Gislason and A. D. Jorgensen**, 1973. Determination of potassium ion-small molecule potentials from total cross section measurements, *J. Chem. Phys*., **78**, 5279-5286.

[101] **Soldan, P., Lee, E.P.F., Wright, T.G**, 1998, Interaction energies of the Na+center dot Rg complexes (Rg = He, Ne and Ar): Basis set considerations for Na+, *J. chem. Soc. Faraday Trans*, **94**, 3307-3318.

[102] **Burns, K.L., Bellert, D., Leung, A.W.K., Breckenridge, W.H., 2001.** M^+/Rg bonding: The effects of M^+ permanent quadrupole moments (M^+ = atomic metal ion; Rg=rare gas atom), *J. Chem. Phys*., **114**, 7877-7890.

[103] **Leung, A.W.K., Julian, R.R., Breckenridge, W.H**, 1999. Potential curves for the ground states and some excited states of MgNe, Mg^+Ne, and Mg^+ ^{2}Ne van der Waals complexes, *J.Chem.Phys.*, **110**, 8443-8455.

[104] **Leung, A.W.K., Julian, R.R., Breckenridge, W.H**, 1999. Potential curves for several electronic states of the MgHe, Mg^+He, and Mg^{+2}He van der Waals complexes, *J.Chem.Phys*., **111**, 4999-5012.

[105] **Massick, S., Breckenridge, W.H**, 1996. Doubly excited valence states of neutral van der Waals molecules: Mg($3p\pi$,$3p\pi$ ^3P_J)·Ar($^3\Sigma^-$), *J.Chem.Phys*., **105**, 6154-6171.

[106] **Moszynski, R., Wormer, P. and Viehlandt**, **L.A., 1994.** The interaction potential and transport coefficients of Na+ ions in the He gas. *J. Phys. B, At Mol. Opt. Phys*., **27**, 4933-4941.

[107] **Moszynski, R., Jeziorski, B., Diercksen, G.H.F., Viehland, L.A.,** 1994. Symmetry-adapted perturbation theory potential for the HeK^+ molecular ion and transport coefficients of potassium ions in helium, *J. Chem. Phys.*, **101,** 4697-4712.

[108] **Sebastianelli, F., Bodo, E., Di Paola, C., Baccarelli, I., Gianturco, F.A. and Yurtsever, M.,** 2005. Microsolvation of Li^+ in bosonic He clusters: I. Many-Body effects on the structure of the small aggregates, J. Comput. Mater. Sci. (in press)

[109] **Soldan,** P**., Lee, E. P. F. and Wright T. J., Lozeille, J., Murrell, N.J.,** 2001. High quality interatomic potential for $LiHe^+$, *Chem. Physics Lett.*, **343**, 429-441.

[110] **Viehland, L.A., Soldan, P., Lee, E. P. F. and Wright T. J., Lozeille, J.,** 2004, Spectroscopy of $K^+ \cdot Rg$ and transport coefficients of K^+ in Rg (Rg=He–Rn), *J. Chem. Physics.*, **121**, 341-354**.**

[111] Gaussian 03, Revision C.02, **M. J. Frisch, G. W. Trucks, H. B. Schlegel, G. E. Scuseria, M. A. Robb, J. R. Cheeseman, J. A. Montgomery, Jr., T. Vreven, K. N. Kudin, J. C. Burant, J. M. Millam, S. S. Iyengar, J. Tomasi, V. Barone, B. Mennucci, M. Cossi, G. Scalmani, N. Rega, G. A. Petersson, H. Nakatsuji, M. Hada, M. Ehara, K. Toyota, R. Fukuda, J. Hasegawa, M. Ishida, T. Nakajima, Y. Honda, O. Kitao, H. Nakai, M. Klene, X. Li, J. E. Knox, H. P. Hratchian, J. B. Cross, V. Bakken, C. Adamo, J. Jaramillo, R. Gomperts, R. E. Stratmann, O. Yazyev, A. J. Austin, R. Cammi, C. Pomelli, J. W. Ochterski, P. Y. Ayala, K. Morokuma, G. A. Voth, P. Salvador, J. J. Dannenberg, V. G. Zakrzewski, S. Dapprich, A. D. Daniels, M. C. Strain, O. Farkas, D. K. Malick, A. D. Rabuck, K. Raghavachari, J. B. Foresman, J. V. Ortiz, Q. Cui, A. G. Baboul, S. Clifford, J. Cioslowski, B. B. Stefanov, G. Liu, A. Liashenko, P. Piskorz, I. Komaromi, R. L. Martin, D. J. Fox, T. Keith, M. A. Al-Laham, C. Y. Peng, A. Nanayakkara, M. Challacombe, P. M. W. Gill, B. Johnson, W. Chen, M. W. Wong, C. Gonzalez, and J. A. Pople**, Gaussian, Inc., Wallingford CT, 2004.

[112] **Lee Roy**, 2001. University of Waterloo Chemical Physics Research Program Report CP-555R.

[113] **Bartlett, R. J., Silver**, **D.M.,** 1975. Many-body perturbation theory applied to electron pair correlation energies. I. Closed-shell first-row diatomic hydrides, *J. Chem. Phys.*, **62**, 3258-3264.

[114] **Pople, J.A., Binkley, J. S., Seeger**, **R.,** 1976. Theoretical models incorparating electron correlation, *Int. J. Quant. Chem., Quant. Chem. Symp.*, **10**, 1-12;

[115] **Pople, J.A., Seeger, R., Krishnan**, **R.,** 1977.Variational configuration interaction methods and comparison with perturbation theory, ibid., *Symp.*, **11**, 149-162.

[116] **Bartlett, R.J., Shavitt**, **I.,** 1977, Comparison of high-order many-body perturbation theory and configuration interaction for H_2O, *Chem. Phys. Lett*., **50**, 190-197.

[117] **Krishnan, R., Pople**, **J.A.,** 1978, Approximate 4th order perturbation theory for electron correlation, *Int. J. Quant. Chem*., **14**, 91-99.

[118] **Levine, I.N., 1991.** Quantum Chemistry, 4. Edition, Prentice Hall, Englewood Cliffs.

[119] **Krishnan, R. , Schlegel, H. B., Pople, J. A., 1980.** Derivative studies in configuration–interaction theory, *J. Chem. Phys.*, **72,** 4654-4662**.**

[120] **Foresman, J. B.,Head-Gordon, M., Pople, J.A., Frisch**, **M.J.,** 1992, Toward a systematic molecular orbital theory for excited states **,** *J. Phys. Chem*., **96**, 135-142.

[121] **Raghavachari, K., Pople, J.A.,** 1981. Calculation of one electron properties using limited configuration interaction techniques, *Int. J. Quant. Chem*., **20**, 167-174.

[122] **Langhoff, S.R., Davidson**, **E.R.,** 1974**.** Configuration Interaction on nitrogen molecule, *Int. J. Quantum Chem.*, **8**, 61-67.

[123] **Krishnan, R., Pople, J.A., Frisch**, **M.J.,** 1980**.** Derivative studies in configuration–interaction theory, *J. Chem. Phys.*, **72**, 4244-4255.

[124] **Raghavachari, K., Pople, J.A.**, 1987. Quadratic configuration interaction. A general technique for determining electron correlation energies, *J. Chem. Phys***., 87**, 5968-5978.

[125] **Coester**,F., 1958. Representation of states in a field theory with canonical variables, *Nucl. Phys.*, ***7***, 421-428.

[126] **Cizek, J.,** 1966. On the Correlation Problem in Atomic and Molecular Systems. Calculation of Wavefunction Components in Ursell-Type Expansion Using Quantum-Field Theoretical Methods, *J. Chem. Phys.*, ***45,*** 4256-4263.

[127] **Raghavachari, K., Pople, J.A., Schlegel, H.B., Binkley**, J.S., 1978. *Int. J. Quant. Chem.*, ***XIV***, 545-550.

[128] **Scuseria, G.E., Janssen, C.L. and Schäfer III, H.F.,** 1988. A systematic theoretical study of harmonic vibrational frequencies: The single and double excitation coupled cluster (CCSD) method, *J. Chem. Phys.*, ***12,*** 7382-7388.

[129] **Urban, M., Noga, J., Cole, S. J. and Bartlett, R. J.,**1985**.** Towards a full CCSDT model for electron correlation, *J. Chem. Phys.*, ***83,*** 4041-4056.

[130] **Pople, J.A. and Head-Gordon, M.,** 1987**.** Quadratic configuration interaction. A general technique for determining electron correlation energies, *J. Chem. Phys*., **87**, 5968-5975.

[131] **Neuhaus, A., Frenking, G., Huber, C. and Gauss**, **J.,** 1992. On the Structure and Existence of CrF_6, *Inorg. Chem*., **31**, 5355-5370.

[132] **J.Labanowski, J. K., Andzelm**, 1991. Density Functional Methods in Chemistry; Eds.; Springer-Verlag: New York.

[133] **Becke**, **A.D.,** 1993. Density-functional thermochemistry. III. The role of exact exchange, *J. Chem. Phys*., **98**, 5648-5658.

[134] **Becke, A. D.,** 1988. Density-functional exchange-energy approximation with correct asymptotic behavior**,** *Phys. Rev. A***, 38**, 3098-3105.

[135] **Lee, C., Yang, W. and Parr, R.G.,** 1988. Development of the Colle-Salvetti correlation-energy formula into a functional of the electron density, *Phys. Rev. B*, **37,** 785-794.

[136] **Stephens, P.J., Devlin, F.J., Chabalowski, C.F. and Frisch**, **M.J.,** 1994. Ab Initio Calculation of Vibrational Absorption and Circular Dichroism Spectra Using Density Functional Force Fields **,** *J. Phys. Chem***., 98**, 11623.

[137] **Woon, D.E. and Dunning Jr., T. H.,** 1993. Gaussian basis sets for use in correlated molecular calculations. III. The atoms aluminum through argon, *J. Chem. Phys.*, **98,** 1358-1367.

[138] **Kendall, R.A., Dunning Jr., T. H. and Harrison**, **R. J.,** 1992. Electron affinities of the first-row atoms revisited. Systematic basis sets and wave functions *J. Chem. Phys.*, **96**, 6796-6803.

[139] **Wilson, A., van Mourik, T. and Dunning Jr**., **T. H.,** 1997**.** *J. Mol. Struct. (Theochem)*, **388**, 339-345.

[140] **Hariharan, P.C. and Pople, J.A.,** 1973. Inluence of polarization functions on molecular hydrogenation energies, *Theoret.Chimica Acta*., **28**, 213-223.

[141] **McGrath, M.P. and Radom**, **L.,** 1991**.** Extension of Gaussian-1 (G1) theory to bromine-containing molecules, *J. Chem. Phys.* **94**, 511-519.

[142] **Ahmadi, G. R., Almlof, J., and Røeggen,** 1995, The interatomic potential for the $X^1\Sigma^+$ state of $ArNa^+$, $NeNa^+$ and $HeNa^+$, *Chem. Phys*., **199**, 33-39.

CURRICULUM VITAE

PERSONAL DETAILS:

Name: Erol YILDIRIM/ M.Sci. student in İstanbul Technical University
DOB: 25-12-1980

EDUCATIONAL QUALIFICATIONS

1992-1995 Anatolian High School / Diyarbakır
1992-1996 1995-1998 Science High School / Diyarbakır
1998-2003 Bilkent University Chemistry Department/ Ankara
2004 Istanbul Tech. University Chemistry Department/ M.Sc. student